



Schweizerische Eidgenossenschaft
Confédération suisse
Confederazione Svizzera
Confederaziun svizra

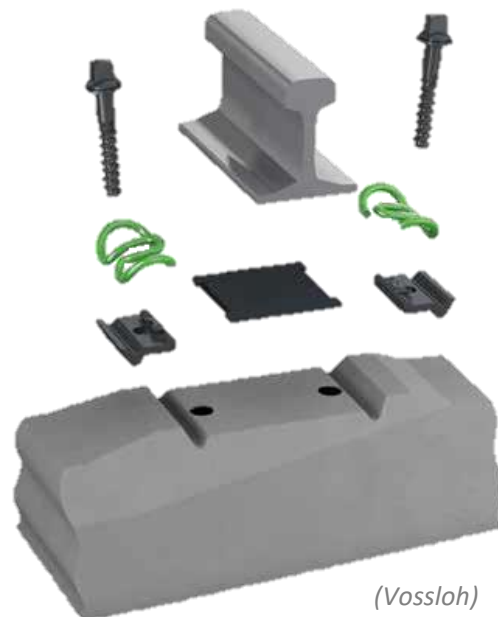


COMATEC
Institut de Conception
mécanique et
Technologies des
matériaux

Commissioned by the Swiss Confederation

Study of rail clamps preload influence on ballast solicitation and acoustic emissions

Final Report



Authors:

Prof. Joël Cugnoni, Maurice Amman, Raphaël Nardin, Vincent Crausaz

August 2021

IMPRESSUM

Commissioned by: Federal Office for the Environment (FOEN) and Federal Office of Transports (FOT), CH-3003 Bern. The FOEN and the FOT are agencies of the Federal Department of the Environment, Transport, Energy and Communications (DETEC).

Contractor: School of Management and Engineering Vaud (HEIG-VD), Institute of mechanical design and materials technology (COMATEC)

Authors: Prof. Joël Cugnoni, Maurice Amman, Raphaël Nardin, Vincent Crausaz

FOEN / FOT support: Franz Kuster, Fredy Fischer, Robert Attinger, Christoph Dürig

Note: This report was undertaken on behalf of the Federal Office for the Environment (FOEN) and the Federal Office of Transports (FOT). The contractor bears sole responsibility for its content.

Abstract

The present report studies the influence of rail clamps loosening on railway noise emissions. Indeed, in addition to loosening over time, clamps are initially not all equally tightened (a previous study conducted by the FOEN found out that about 15% of clamps were incorrectly tightened). This implies that all rail pads are not subjected to the same preload. Consequently, their tangent stiffness is not uniform along the rail track and it is expected to have an effect on its dynamics, thus on noise disturbances.

Vibratory and acoustic measurements were performed on a three-sleeper unit cell, where the ballast was replaced by equivalent wooden beams. It was excited at the tip of one rail by a shaker fed with a white noise signal, at an angle of 45° with respect to the vertical direction and pointing inward. Experiments were conducted with both hard and soft EVA pads, the former consisting of a simple plate and the latter having a textured pattern. A vibro-acoustic finite element model of the three-sleeper unit cell was developed as well. It allowed computing the radiated acoustic power spectrums and the accelerance at some specific points of the setup. Results were analysed in the frequency range from 300Hz to 1500Hz.

Various scenarios were investigated: in the first one, the preload of all twelve clamps was reduced to 75%, 50%, 25% and 0% of the nominal preload (100%, 9kN). In the second scenario, the preload of 1, 2 and 4 clamps on the middle sleeper were reduced to 50%, all other clamps remaining fully tightened.

Concerning the first loading scenario, the experiments showed that decreasing the clamps preloads has no significant effect unless they are completely untightened, in which case an increase in noise emissions of 2dB was measured. On the other hand, the linear nature of simulations showed that decreasing the clamps preloads gradually increases the noise emissions up to 2.8dB when the clamps are fully loose.

As for the second loading scenario, experimental and numerical results showed that setting the preloads of 8%, 16% or 33% of the clamps to 50% of the nominal preload has only a very little influence on the radiated noise level for both pad types. No clear difference was measured in the experimental part, while the model predicts noise emissions increase of up to 0.5dB for hard EVA pads, which can be considered negligible compared to the effect of other factors.

Table of contents

1	Introduction.....	4
2	Project goals and deliverables.....	5
2.1	Goals.....	5
2.2	WP1: Experimental measurements.....	5
2.3	WP2: Numerical simulations.....	5
3	WP1: Experimental measurements.....	6
3.1	Unit-cell presentation.....	6
3.2	Experimental scenarios.....	7
3.3	Vibratory measurements.....	9
3.4	Acoustic measurements.....	12
3.5	Impact tests.....	17
4	WP2: Simulation models.....	19
4.1	FE model presentation.....	19
4.2	Numerical scenarios.....	20
4.3	Harmonic results.....	20
4.4	Acoustic results.....	24
5	Discussion & conclusion.....	30
5.1	Synthesis.....	30
5.2	Conclusion.....	31
6	References.....	33
7	Appendices.....	34
7.1	Clamp preload adjustment.....	34
7.2	Vibratory measurements.....	35
7.3	Acoustic measurements.....	36
7.4	Impact measurements.....	37
7.5	Simulations.....	38

1 Introduction

The Federal law about the reduction of railways noise emissions (DE: Bundesgesetz über die Lärmsanierung der Eisenbahnen, BGLE (1)) states that 2/3 of people subject to railway noise must be protected from said emissions. The protective measures must be applied in priority to the rolling material and to the railway tracks, and then to the sound propagation pathways. Part of the funding is also to be invested in research projects to study and develop technologies aiming to reduce railway noise emissions.

A research project (2) conducted by the FOEN and KPZ Farhbahn AG in 2021 found out that approximately 15% of railway fixation clamps were not properly tightened.

The aim of the present research project is to evaluate, experimentally and numerically, the influence of incorrect rail clamp tightening on the acoustic emissions of the railway, in order to determine if it could be the subject of further research or noise reduction measures. The influence of incorrect tightening on vibrations is also to be evaluated.

2 Project goals and deliverables

2.1 Goals

The goal of the project is to evaluate the influence of rail clamps tightening on acoustic emissions and vibrations. This is done experimentally and numerically.

2.2 WP1: Experimental measurements

The experimental measurements of the vibratory and acoustic behaviour were done on a three-sleeper unit-cell that was developed and used in the FOEN project *Novel Rail Pads for Improved Noise Reduction and Reduced Track Maintenance*¹. Vibratory and acoustic measurements were conducted for various scenarios, representing different clamp tightening levels and different occurrences of incorrect tightening. The measurements were conducted with hard and soft EVA pads from SBB

2.3 WP2: Numerical simulations

The numerical FE model which was developed in the FOEN project mentioned above was adapted to the current project. It is the digital twin of the experimental three-sleeper unit-cell and allows performing vibratory and acoustic computations. Practically the same scenarios as in the experimental measurements (except that EVA soft was not included) were simulated with this model and some further analyses were done as well.

¹ <https://www.aramis.admin.ch/Texte/?ProjectID=44161>

3 WP1: Experimental measurements

3.1 Unit-cell presentation

The measurements were performed on a unit-cell consisting of:

- three B91 sleepers (without undersleeper pads)
- two 60E1 rails, 1.80m long
- six hard EVA pads, 7mm thick
- six soft EVA pads, 7mm thick
- twelve Vossloh W 14 clamping system, consisting of Skl 14 clamps, Wfp 14K angle guide plates, Ss 0 sleeper screws and Uls 7 washers

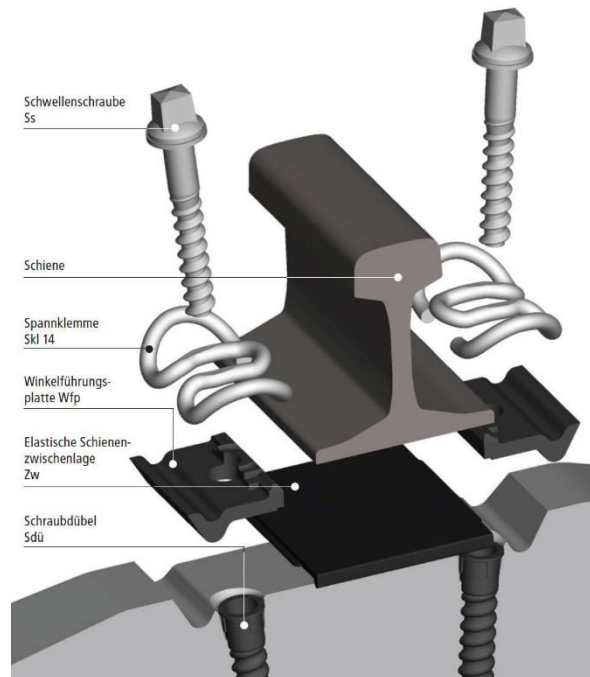


Figure 1 - Vossloh W 14 clamping system (source: Vossloh)



Figure 2 - Hard (left) and soft (right) EVA railpads

The setup is placed on an equivalent ballast structure made of 10cm thick wooden beams (spruce). For both vibratory and acoustic measurements, the setup is excited by a B&K V406 electromagnetic shaker attached at the end of a rail at an angle of 45° (see image below). This shaker is fed a white noise signal in order to excite a wide frequency spectrum in the range of interest corresponding to the rail and sleeper vibrations (300 to 1500 Hz).



Figure 3 – The three-sleeper unit-cell setup



Figure 4 - B91 sleeper with a hard EVA pad and the W14 clamping system

3.2 Experimental scenarios

The Wk 14 clamps are designed for a nominal preload of 9kN. The preload can be set by adjusting the tightening of the sleeper screw. Various preload levels and occurrences scenarios have been investigated.

The first scenario that was tested was with all twelve clamps of the setup preloaded at 100, 75, 50, 25 and 0% of the nominal preload (100% being fully tightened, and 0% totally loose), with hard EVA pads installed. The goal was to get results for boundary situations (totally tightened clamps vs totally loosened clamps).

The 50% preload scenario was then investigated, with both hard and soft EVA pads, for various occurrences of 8, 16 and 33% (respectively one, two and four clamps out of twelve). Based on the illustration below, 8% correspond to the n°5 clamp loaded at 50%, 16% to the clamps 5 & 6 and 33% to the clamps 5, 6, 7 & 8, while all other clamps are tightened at 100%.

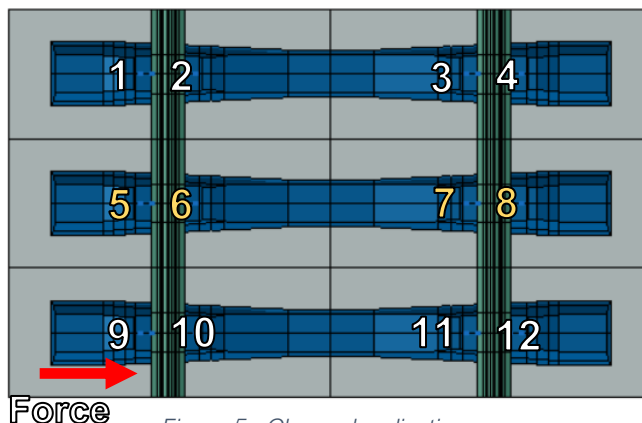


Figure 5 - Clamps localisation

The affected clamps were chosen on the central sleeper, so the rail behaviour is closer to the one of an actual railway track, which are continuous and do not have loose ends. The 50% preload level was chosen because it represents a realistic case of incorrect tightening (totally loosened clamps being obviously very rare).

In summary, the following scenarios were tested:

Hard EVA:

- All clamps preloaded at 100, 75, 50, 25 and 0% of the nominal preload
- 1, 2 and 4 clamps (8, 16, 33%) on the central sleeper loaded at 50% of the nominal preload.

Soft EVA:

- 1, 2 and 4 clamps (8, 16, 33%) on the central sleeper preloaded at 50% of the nominal preload.

To refer to these various scenarios throughout the different charts and graphs, a naming convention was used. This states the type of pad (EVAHARD, EVASOFT), the occurrence of the preload (8, 16, 33%) and the preload level (100, 75, 50, 25 and 0%).

For example:



means the measurement was made with EVA hard pad, with 33% (i.e. 4/12) of the clamps preloaded at 50% of the nominal preload. The remaining 67% (8/12) of the clamps are fully tightened.

The methods used to set the preloads are detailed in the appendices.

3.3 Vibratory measurements

3.3.1 Vibrations and noise emissions

A brief description of the vibratory measurement method is given in the appendices as well as the location of all measured points.

Noise emissions are closely linked to the level of vibrations. Indeed, noise is produced when the surface of a body oscillates at a certain speed. The easiest way to measure the amplitude of vibration is to measure the acceleration. If a given surface has a greater amplitude of acceleration, it will also have greater noise emissions.

In the following graphs, the accelerance is presented, which is the acceleration divided by the input force.

3.3.2 EVA hard – all clamps with various preloads

The Figure 6 shows the amplitude of accelerance (acceleration normalized by the input force) for various degrees of clamp tightening, from fully tightened (100%) to fully loose (0%). The amplitudes are in the lateral direction (parallel to the sleepers), on a point of measurement on the excited rail between two sleepers (point 30, see appendices).

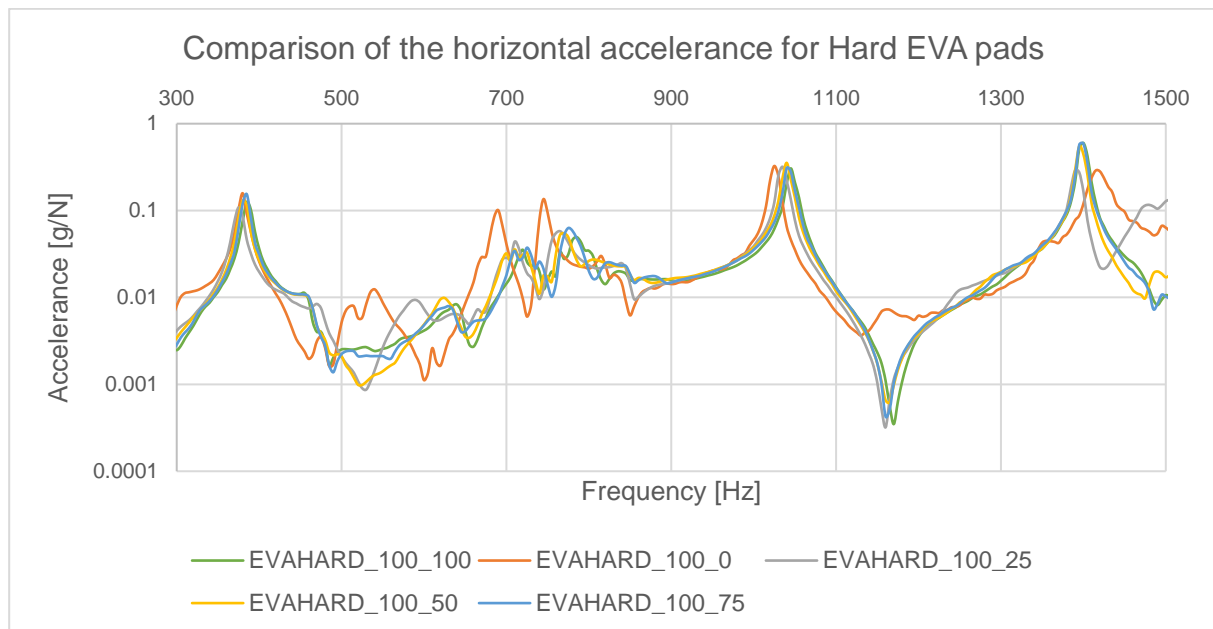


Figure 6 - Comparison of the horizontal accelerance for Hard EVA pads with various preloads

As one can see, all the curves, except the orange one (fully loose), follow the same path. Down to 25% of the nominal tightening force, the accelerance does not seem to be affected, but once the clamps are fully loose the amplitude increase significantly. Especially on the frequency range of 450 Hz to 850 Hz.

The Figure 7 shows the same plot in the vertical direction.

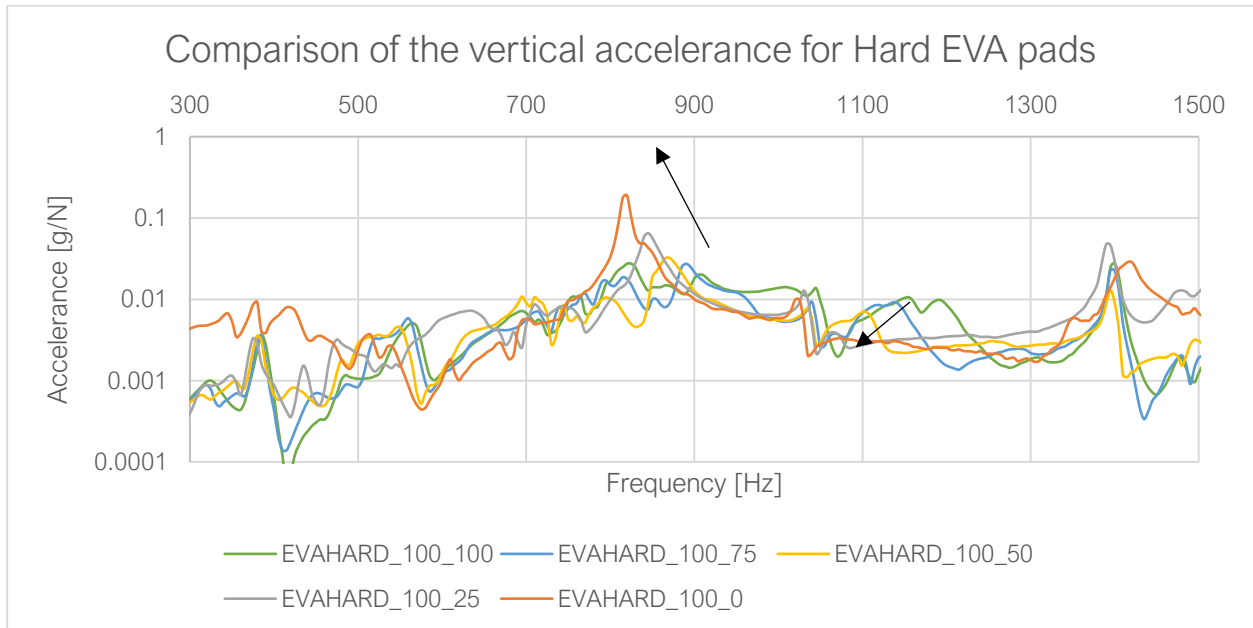


Figure 7 - Comparison of the vertical acceleration for Hard EVA pads with various preloads.

In this case, vibrations at low frequency (300-500Hz) follow the same pattern as previously. However, at higher frequency, the shift in amplitude is spread over the degree of tightening. One can see that the peak around 850 Hz increases in amplitude and decreases in frequency as the clamp becomes looser.

A different behaviour can be observed between 1100Hz and 1300Hz : the amplitude and the frequency decrease when the clamps are looser.

3.3.3 EVA hard & soft – various occurrences of a 50% preload

The next measurements focus on more realistic tightening cases: 8, 16 and 33% of the clamps being half-loose (50% of the nominal load). As there are 12 clamps, this means 4, 2 or 1 untightened clamp(s).

As one can see on the Figure 8 and Figure 9, for hard and soft EVA pads, no differences in terms of vibrations are present. The data shown here comes from the measurement points 30 and 31 respectively, but this is also the case for other points and directions.

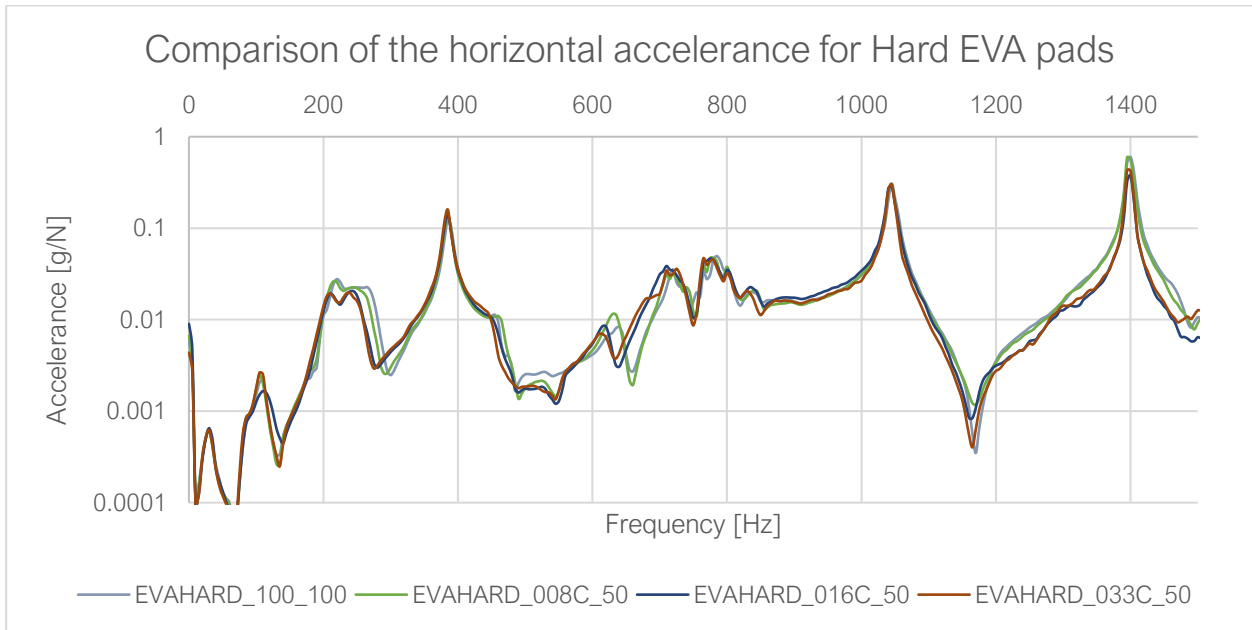


Figure 8 - Comparison of the horizontal acceleration for Hard EVA pads and partial unloading.

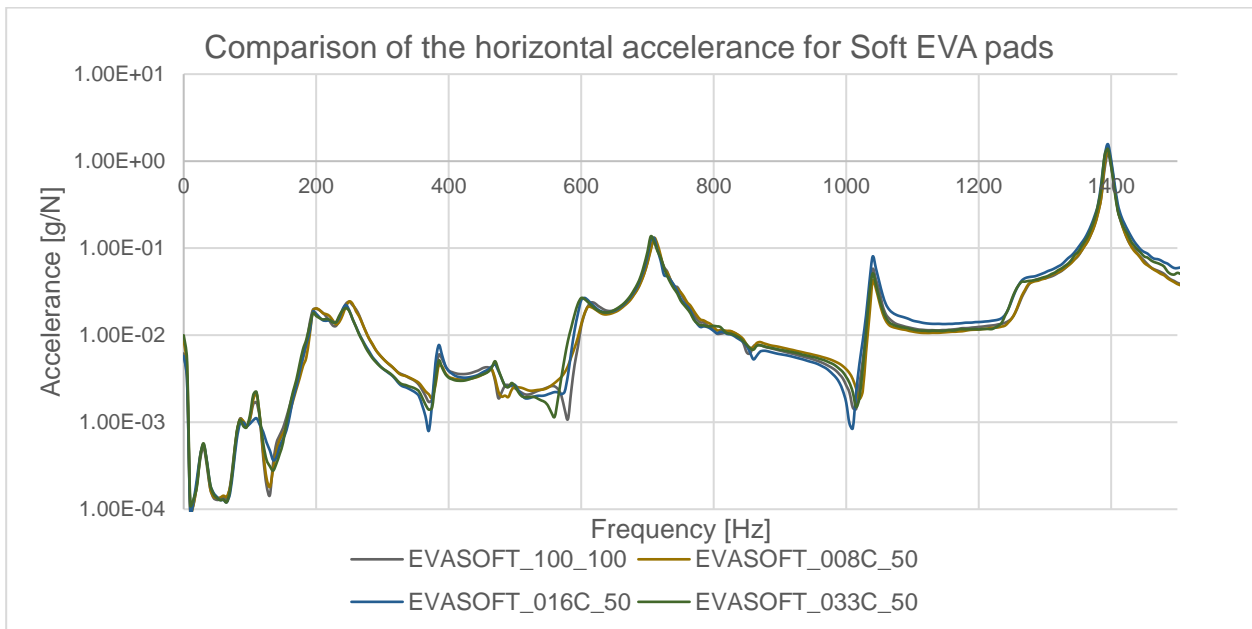


Figure 9 - Comparison of the horizontal acceleration for Soft EVA pads and partial unloading.

3.4 Acoustic measurements

3.4.1 Measurement technique

The acoustic measurements were performed with a pair of microphones, moved all around the unit-cell by a semi-automated 3-axis gantry (see images below). The radiated acoustic intensity was measured all around a virtual “box” enclosing the unit-cell and integrated over the surface to measure the radiated acoustic power. This acoustic power is normalised by the exciting force squared, to allow for comparison between different measurements, as the exciting force may vary slightly.

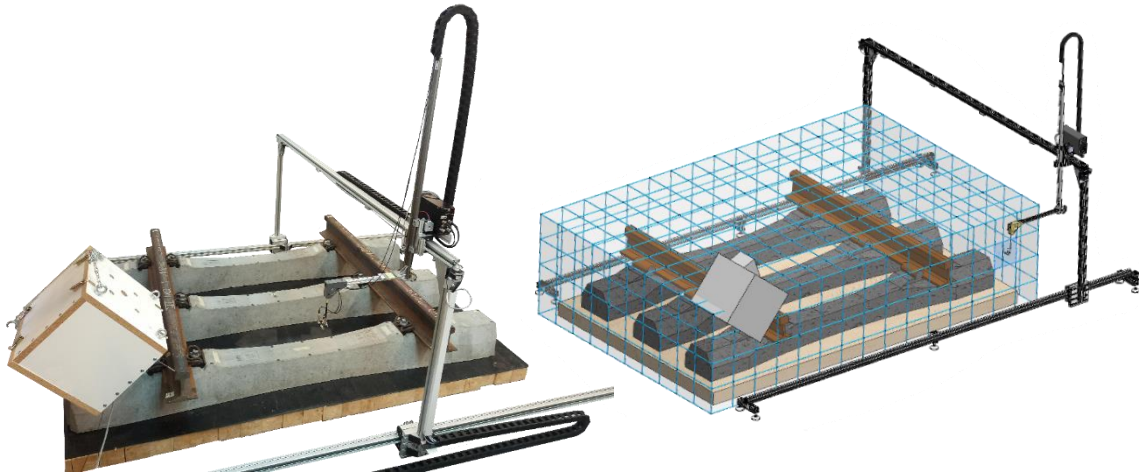


Figure 10 - The unit-cell with the 3-axis gantry (left), representation of the measurement "box" (right)



Figure 11 - Pair of microphones for intensimetry measurements

The acoustic results are given in two graphs: one is a plot that shows the radiated power over the 300-1500Hz frequency range. To further analyse certain parts of the spectrum, some frequency bands are highlighted. The power levels of these discrete bands are represented in bar graph for easier visualization. The values are given in decibels (dB) of W/N^2 . Although these values cannot be compared with other usual acoustic dB scales such as dB(A), *the difference between two values of the bar graph is the same as the difference between two values in the dB(A) scale*. Based on the repeatability and precision of the measurements, the frequency range from 350Hz to 1100Hz will principally be considered, as it is more reliable (high coherence indicator, as the size of the error bars of the bar graph show).

More technical details about the acoustic measurements are given in the appendices.

3.4.2 EVA hard – all clamps with various preloads

The following graphs show the results for various preload levels applied to *all twelve clamps*, with hard EVA pads.

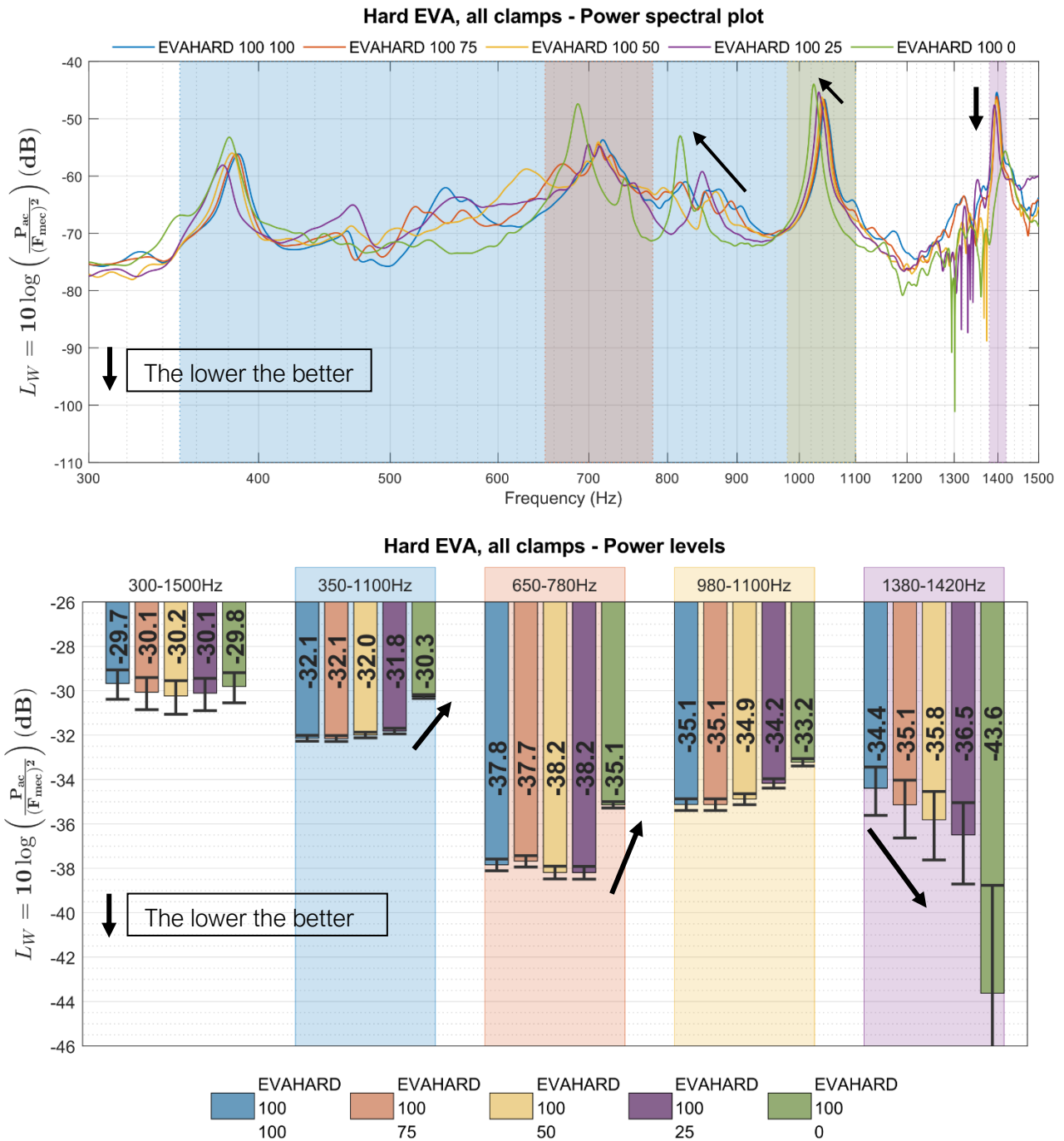


Figure 12 - Spectral (top) and bar graph (bottom) view of the radiated acoustic power, for various preloads applied to all clamps, with hard EVA pads

The acoustic behaviour follows similar trends as the vibratory results. As the clamps are loosened, a downward frequency shift of the peaks can be observed, as well as an increase of amplitude of the peaks around 700Hz and 1000Hz and a decrease of amplitude of the peak at 1400Hz. When looking at the bar graph, it appears that from 100% down to 25% of preload, there is no significant influence on acoustics, the noise emissions only get louder for a 0% preload. The 1400Hz peak behaves the opposite way: it gets quieter with a 0% preload. This peak also seems to show a downward trend the looser the clamps get, but the significance of this effect is limited as this frequency band is hard to excite with this setup and the uncertainty is significant for this resonance peak.

3.4.3 EVA hard – various occurrences of a 50% preload

The following graphs show the results for a preload of 50% applied to one, two and four clamps, with hard EVA pads.

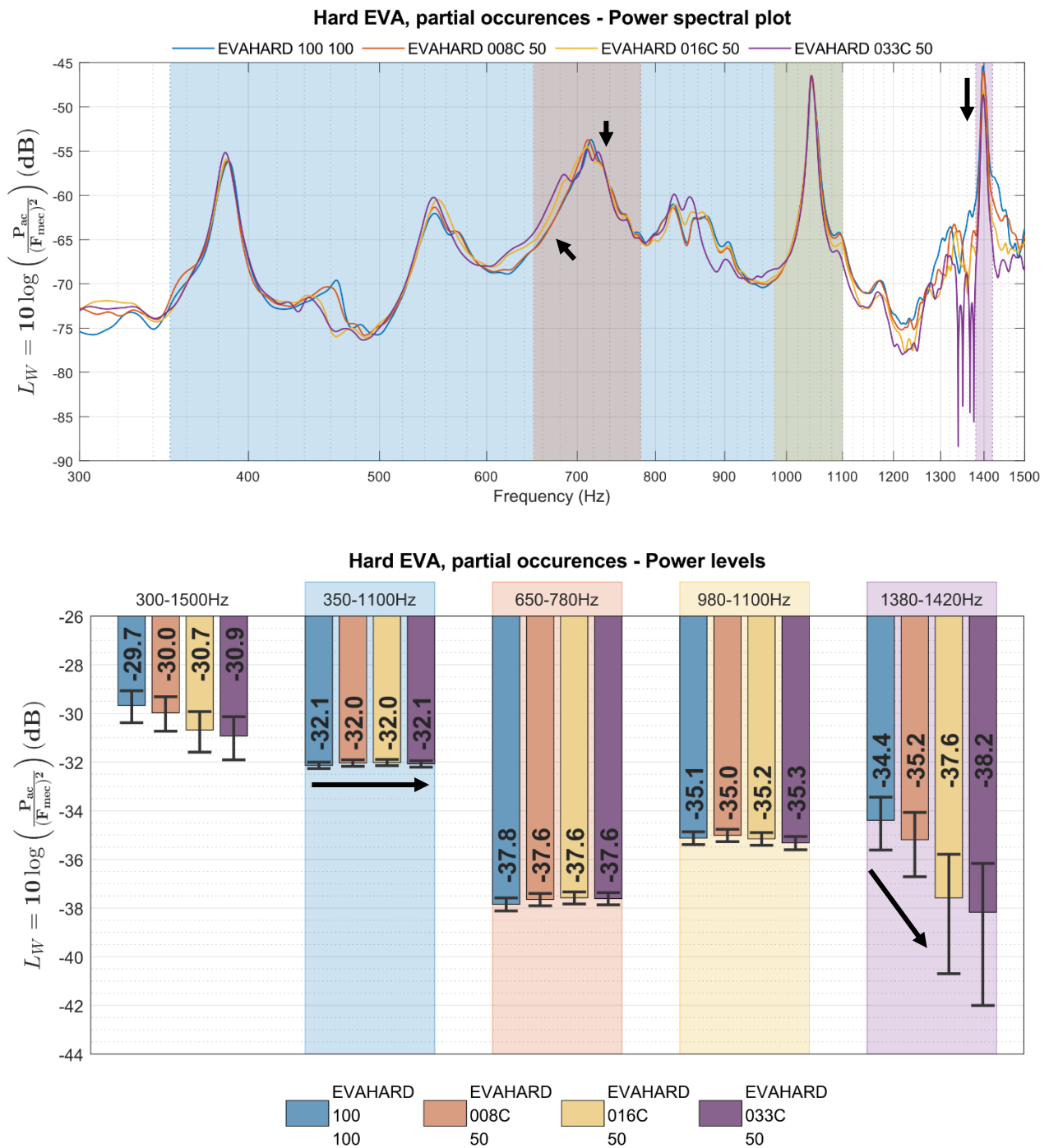


Figure 13 - Spectral (top) and bar graph (bottom) view of the radiated acoustic power, for a 50% preload applied to a various number of clamps, with **hard** EVA pads

When looking at the spectral view, all four curves appear similar. The peaks at 700Hz and 1400Hz show a small decrease in amplitude, as more clamps are preloaded at only 50%. When looking at the bar graph, the levels of the 300-1500Hz range seem to decrease. However, this appears to be mostly driven by the 1400Hz peak, which also adds more uncertainty to the results. The results in the 350-1100Hz are more reliable and *don't show any significant difference between the various loading cases.*

3.4.4 EVA soft – various occurrences of a 50% preload

The following graphs show the results for a preload of 50% applied to one, two and four clamps, with hard EVA pads.

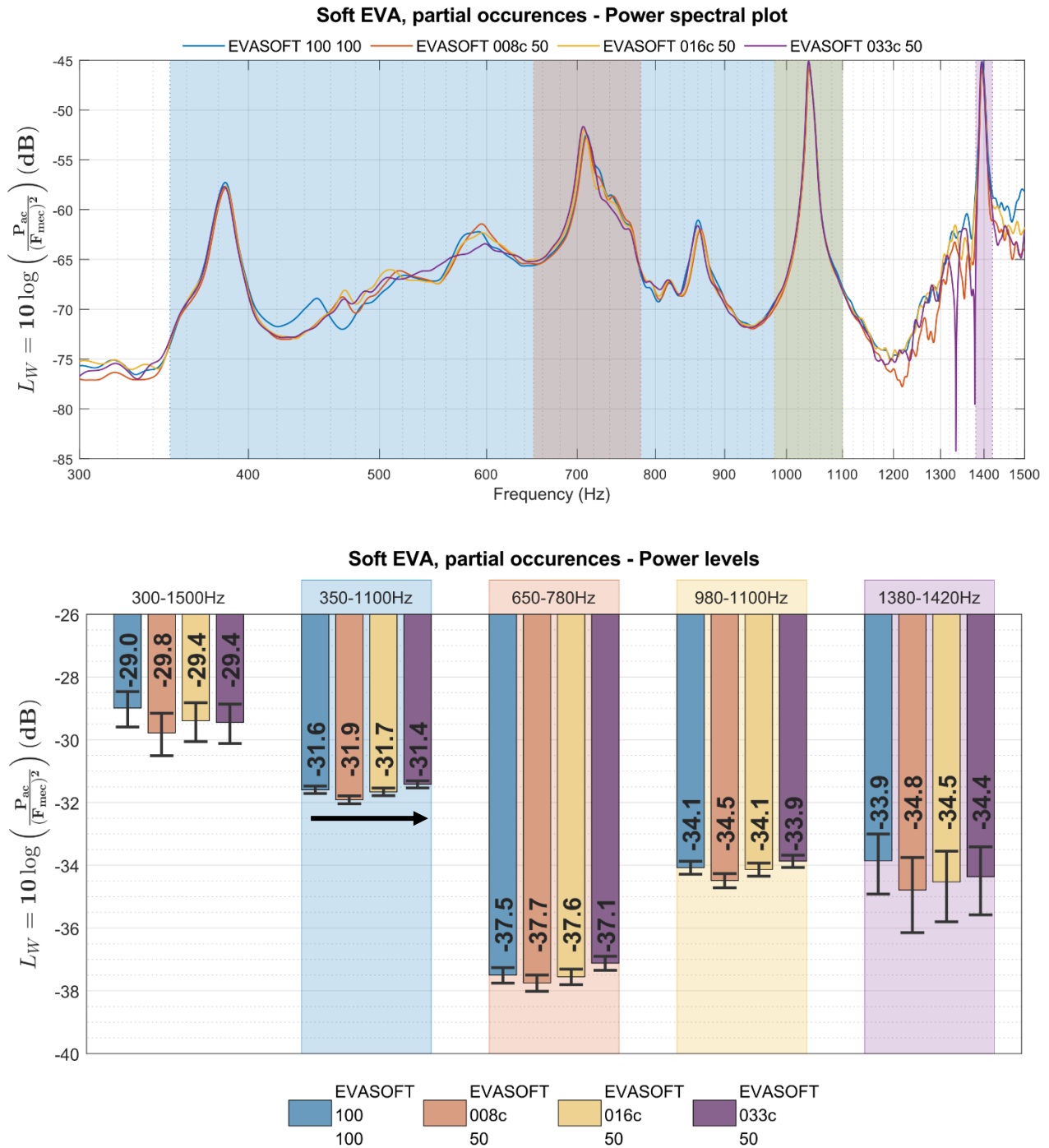


Figure 14 - Spectral (top) and bar graph (bottom) view of the radiated acoustic power, for a 50% preload applied to a various number of clamps, with **soft** EVA pads

With soft EVA pads, there is no visible trend on the spectral plot, as all curves are similar. On the bar graph, the radiated noise seems to get slightly louder as more clamps are unloaded. *However, this trend is not significant enough as it stays within the range of the error bars.*

3.4.5 5.7° excitation

After the first batch of measurements, a setup designed to excite the rail at an angle of 5.7° instead of 45° was made available. This way to excite the rails is closer to the solicitation of an actual railway track as it corresponds to the estimate of 10% of lateral loading vs vertical loading that has been determined during pass-by measurements by performed by EMPA. Some more measurements were then made to assess if the clamping preload has more influence under this loading. The investigated clamping scenarios were:

- All clamps fully tightened
- Only the four central clamps preloaded at 50%, with the rest of the clamps fully tightened
- All clamps preloaded at 50%

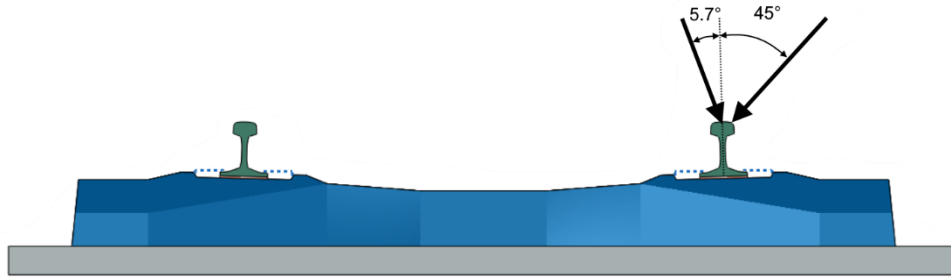
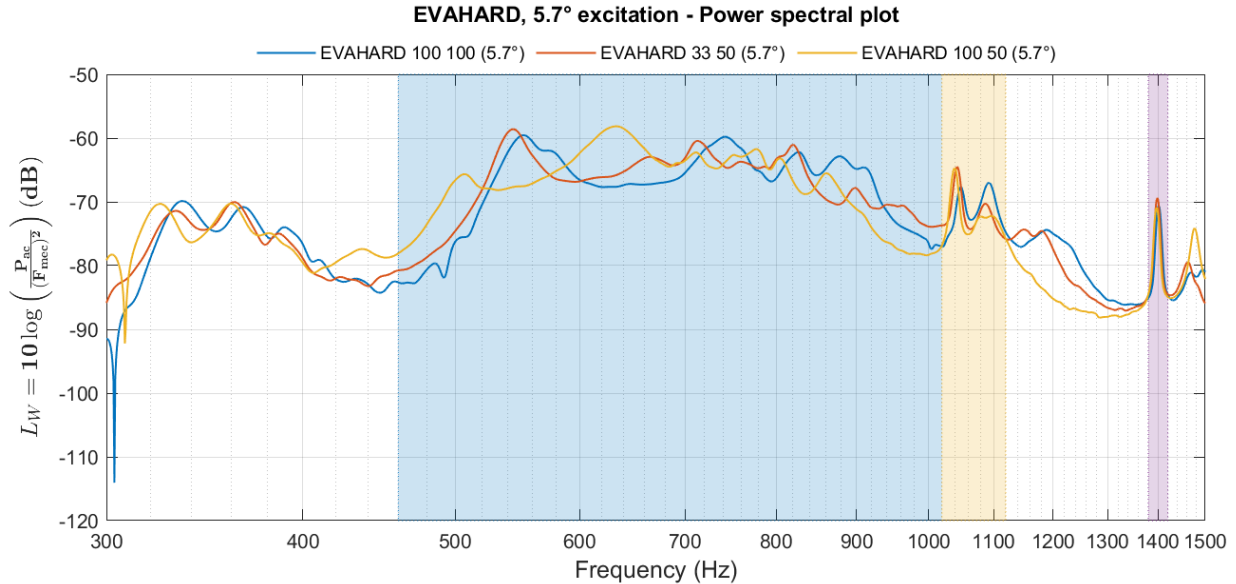


Figure 15 - Illustration of the 5.7° loading

The results can be seen on Figure 16. As for a 45° loading, the clamp preload does not have significant influence on the overall radiated noise. Some variations can be observed on the peaks around 1060Hz and 1400Hz, but since the majority of the noise is radiated in the 460-1000Hz range and since the level of these peaks are below those of this range, these variations have an overall negligible effect on the total radiated acoustic power.



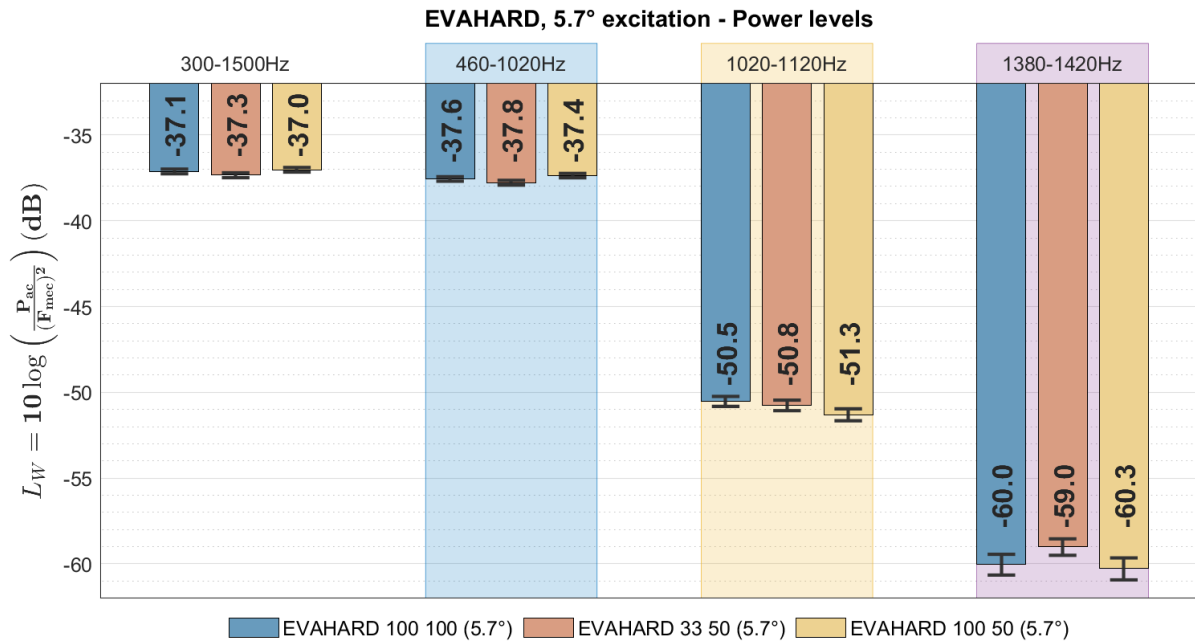


Figure 16 - Spectral (top) and bar graph (bottom) view of the radiated acoustic power, for a 50% preload applied to only the four central clamps or all the pads,, with an excitation at 5.7°

3.5 Impact tests

3.5.1 EVA hard – all clamps with various preloads

Impact tests have been done on the unit-cell. These allow to measure the displacement of specific points following an impact on the rail. Some more information about this test can be found in the appendix.

The Figure 17 shows the peak to peak displacement amplitude of the concrete slab under the unit-cell after an impact. As one can see there is no significant difference whether the clamps are preloaded at 100%, 75%, 50% or 25%. However, the displacement when the clamps are loose (0% preload) is greater than for previous cases.

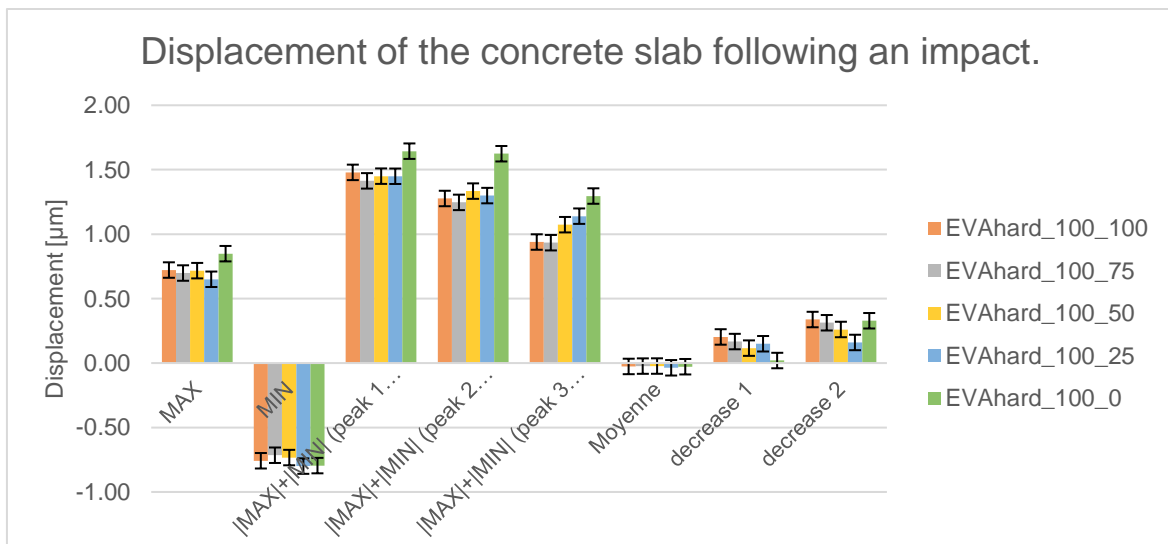


Figure 17 - Displacement of the concrete slab following an impact for various preloads (EVA hard pads).

3.5.2 EVA hard & soft – various occurrences of a 50% preload

In the case of partial unloading, there is no significant differences between the loading cases when EVA hard pads are in place, see Figure 18, except eventually a slight increasing trend when the clamps are loose.

When EVA soft pads are in place, the test with 16% of the clamps at 50% load is slightly lower than expected. This result does not follow the expected behaviour of the system. Indeed, when compared with the results of the EVA hard pads or with the other types of tests, vibrations and acoustic, the 16% preload test should be between the 8% and 33% tests, not lower than both. It is probable that during the test, a problem that slightly changes the measurement at 16% occurred. If this problem is put aside, the same behaviour as for hard pads is present: no significant differences, eventually a slight increase with loose clamps.

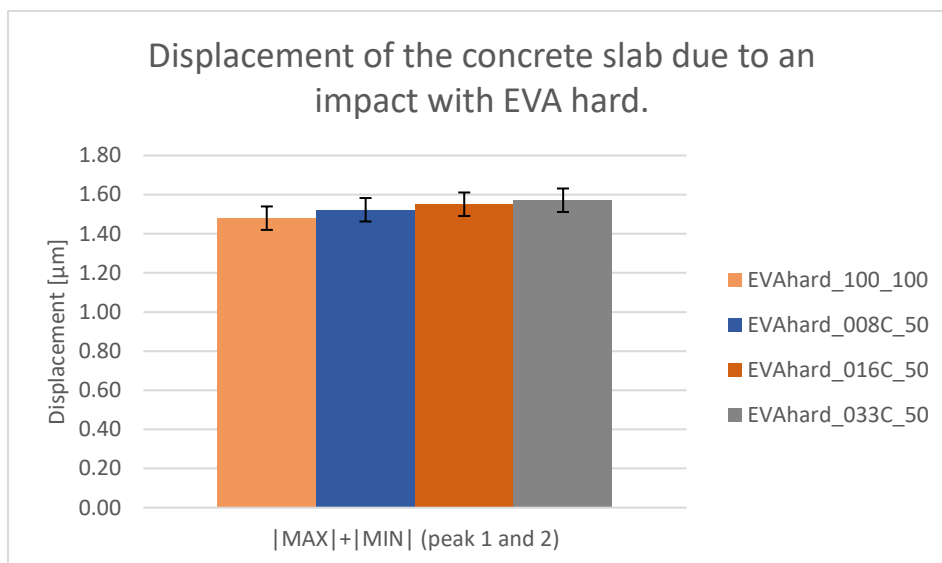


Figure 18 - Displacement of the concrete slab due to an impact, EVA hard pads.

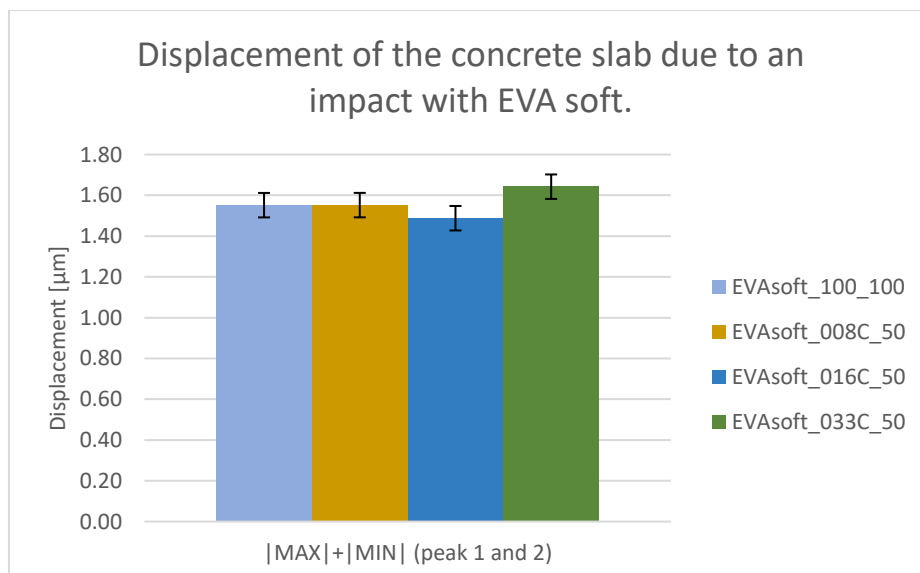


Figure 19 - Displacement of the concrete slab due to an impact with EVA soft.

4 WP2: Simulation models

4.1 FE model presentation

The three-sleeper cell model performs harmo-acoustic simulations of a 1.8-meter-long rail track, which is the digital twin of the actual experimental set-up. It allows studying the influence of various parameters on the dynamic behavior of the system as well as the radiated noise level. Every part is modelled in 3D with few modifications for simulation purposes (removed chamfers and fillets for instance) and the interactions between the components are modelled as perfectly glued contacts.

This model is composed of about 90'000 3D solid elements and 120'000 nodes. All elements have linear shape functions for computational cost purposes. A convergence study was carried out to make sure the results are accurate.

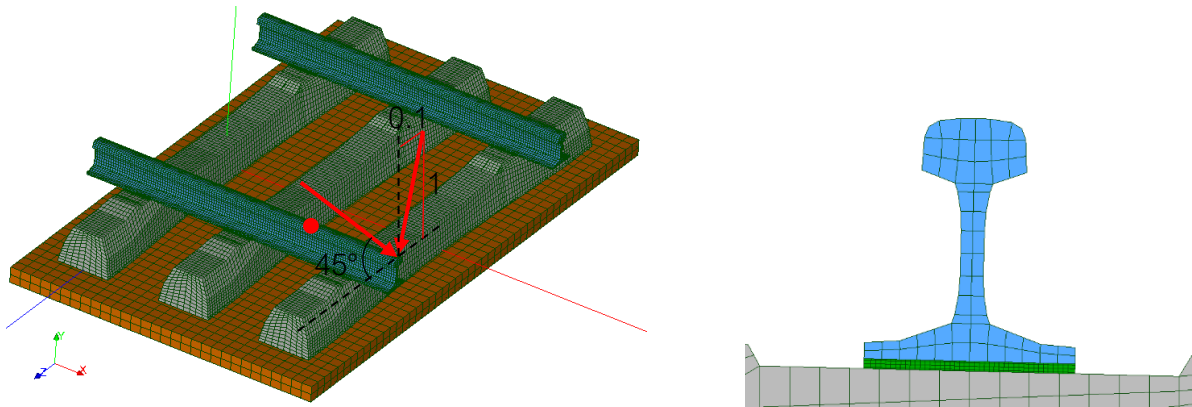


Figure 20 - Mesh of the three-sleeper cell FE model (left) and zoom on a rail-pad-sleeper mesh interaction (right)

All materials are linear, viscoelastic, and only the pads mechanical properties are treated as frequency-dependent (see Appendix 7.5.1). The preloads variations are implemented by tuning the pads Young's modulus, using coefficients that pad compression tests provided (see Appendix 7.5.2).

While the bottom of the wooden "ballast" is fixed, a frequency-independent harmonic force is applied at the tip of one rail (see Figure 20) at an angle of 45° or with a 10% laterally-oriented component, like in the experimental setup. The red point indicates where the acceleration is measured.

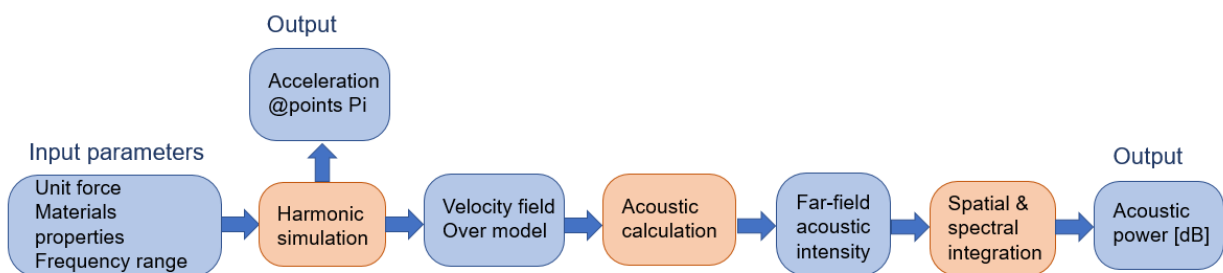


Figure 21 - Diagram of the numerical model operations

The Figure above schematizes how the whole numerical model works. To compute the radiated acoustic power, the pressure field is calculated as a superposition of monopole sources, which compose the radiating surfaces (more details in Appendix 7.5.3).

4.2 Numerical scenarios

The same scenarios as in the experimental part were simulated. However, only hard EVA pads were studied, and all scenarios were also implemented with the 10% lateral force. This force, pointing outward of the track at an angle of $\arctan(0.1) \cong 5.7^\circ$, reflects the actual loading direction during a train pass-by. The scenarios are as follows.

- All clamps preloaded at 100, 75, 50, 25 and 0% of the nominal preload
- 1, 2 and 4 clamps (8, 16, 33%) on the central sleeper loaded at 50% of the nominal preload.

The effect of preload is implemented in the model as a variable pad stiffness depending on the preload level. The effect of preload on the dynamic pad stiffness is estimated based on the tangent stiffness evolution in a quasi static test of the pads (more details are given in appendix).

4.3 Harmonic results

Here are presented the main results of the harmonic analysis: the horizontal and vertical accelerances at the point described previously (Figure 20): on top of the excited rail, between two sleepers.

4.3.1 EVA hard – all clamps with various loads

With the 45° loading (Figure 22 and Figure 23), the trends show that decreasing the preloads increases all peaks magnitudes. However, compared to the experimental results that only showed an effect for completely loose clamps, the effect in the simulations is more progressive with various degrees of preload. A frequency shift of the modes is also observable: indeed, an higher preload means higher pad stiffness, hence higher resonance frequencies for pad dominated modes.

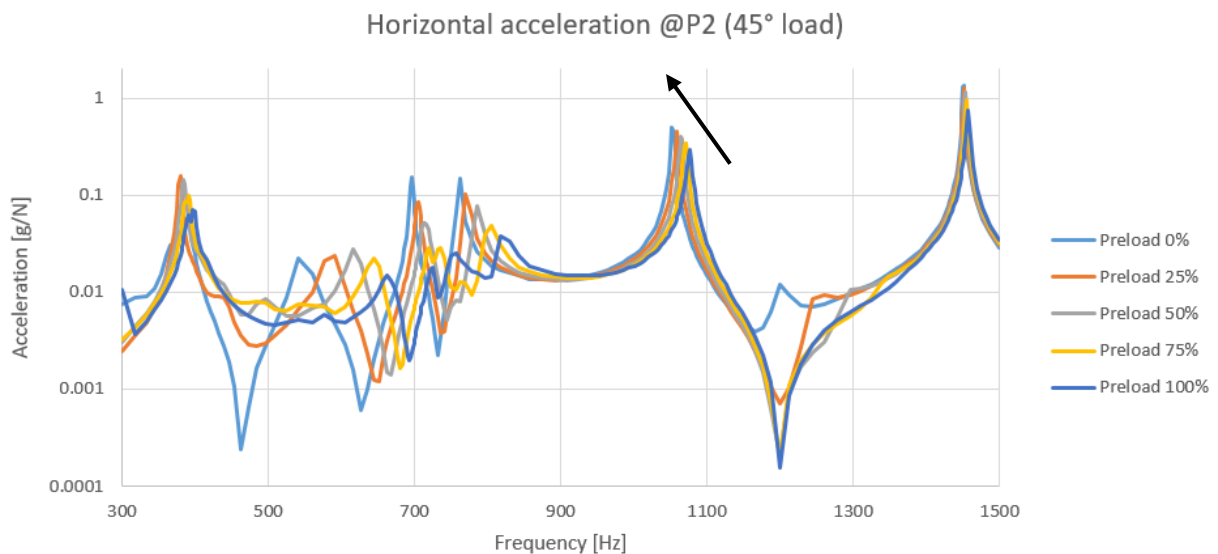


Figure 22 - Horizontal accelerance spectrums with various uniform preloads (45° load)

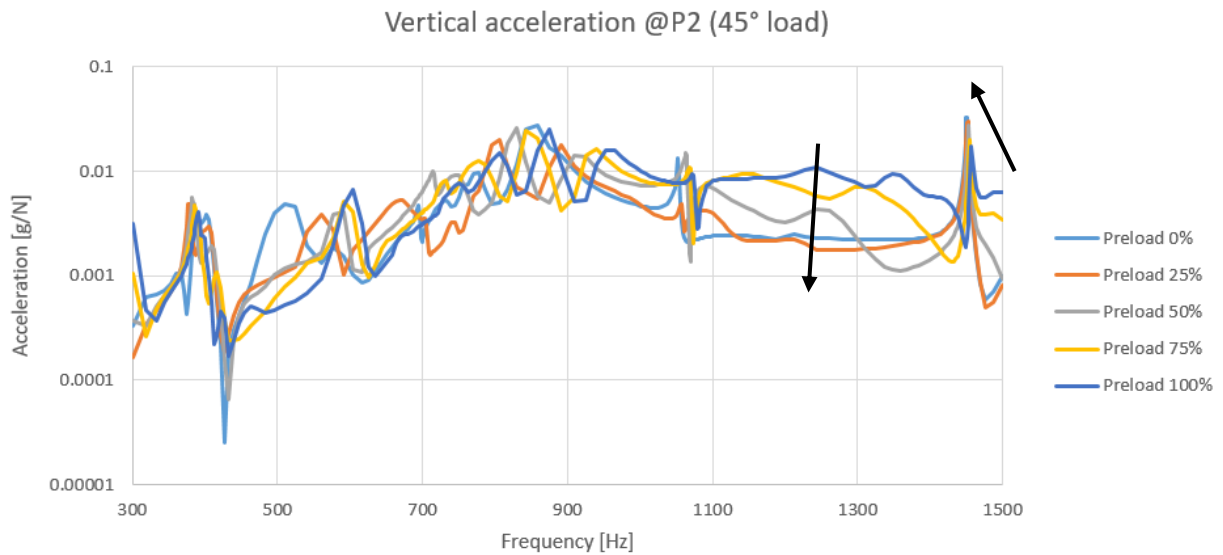


Figure 23 - Vertical accelerance spectrums with various uniform preloads (45° load)

It should be noted that the more progressive effect of preload in the simulated system compared to the abrupt change for the experiment is directly related to the assumptions made for the evolution of the dynamic pad stiffness with preload. In this study, the dynamic pad stiffness is assumed to follow a similar dependence to preload than the quasi-static pad stiffness. The discrepancies of the simulated vs experimental results suggest that in reality, the dynamic pad stiffness is not reduced as much as its static stiffness for lower levels of preload.

With the 5.7° (10% lateral) load (Figure 24 and Figure 25), the same effects are not observable in the whole spectrum. Due to the load direction, vertical modes are obviously more excited. One can see that at high frequencies, decreasing the preload surprisingly seems to decrease the vibrations in a large frequency range.

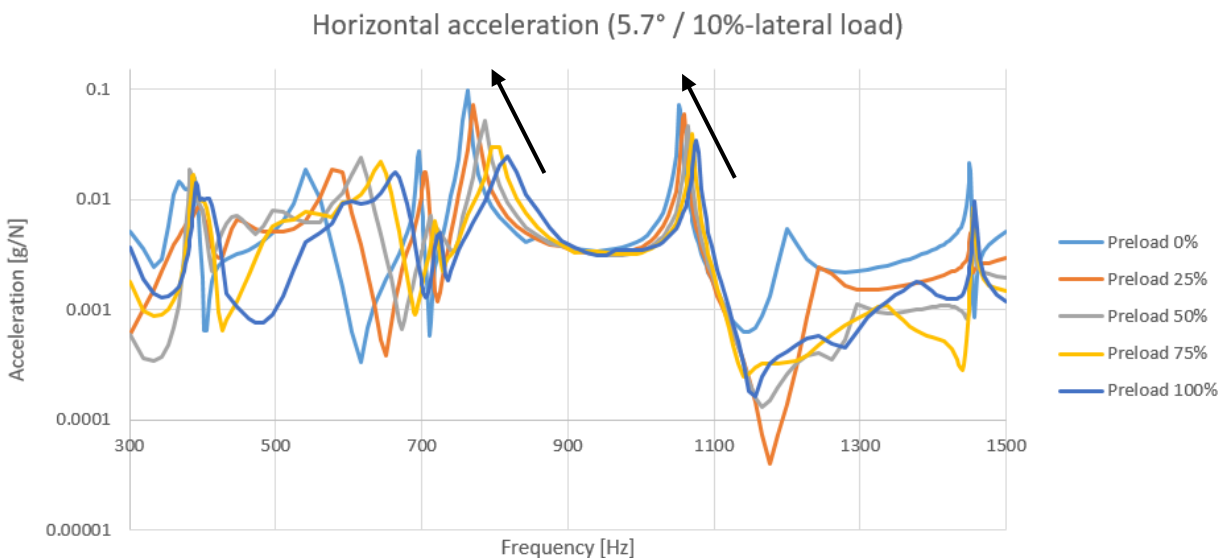


Figure 24 - Horizontal accelerance spectrums with various uniform preloads (5.7° / 10%-lateral load)

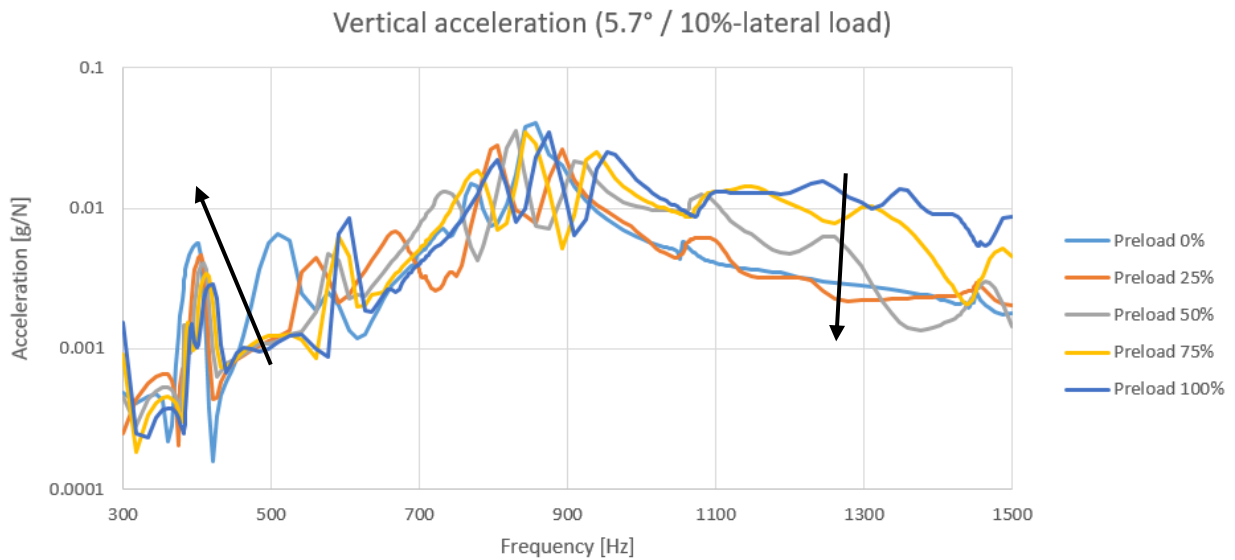


Figure 25 - Vertical acceleration spectrums with various uniform preloads (5.7° / 10%-lateral load)

4.3.2 EVA hard – various occurrences of a 50% preload

Varying the number of clamps that are half-preloaded only slightly influences the acceleration, unless all of them are concerned. The experimental measurements showed the same trend. Since it is difficult to draw conclusions from these raw results, whose curves are very close to each other, a study investigating the emitted acoustic power and the contributions from the components is carried out in 4.4 Acoustic results.

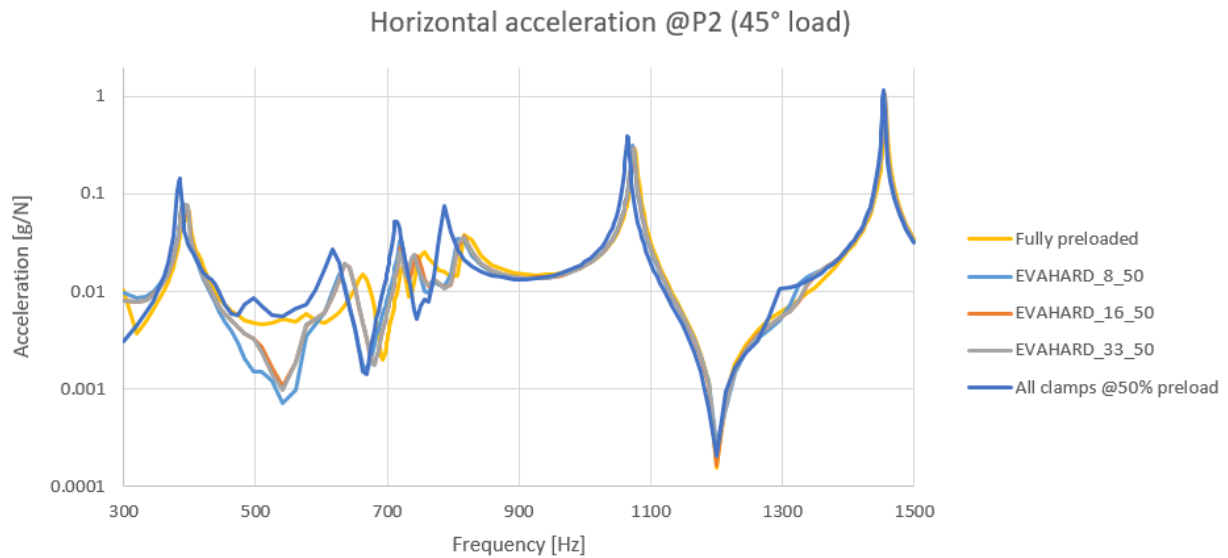


Figure 26 - Horizontal acceleration spectrums when varying the number of half-preloaded clamps (45° load)

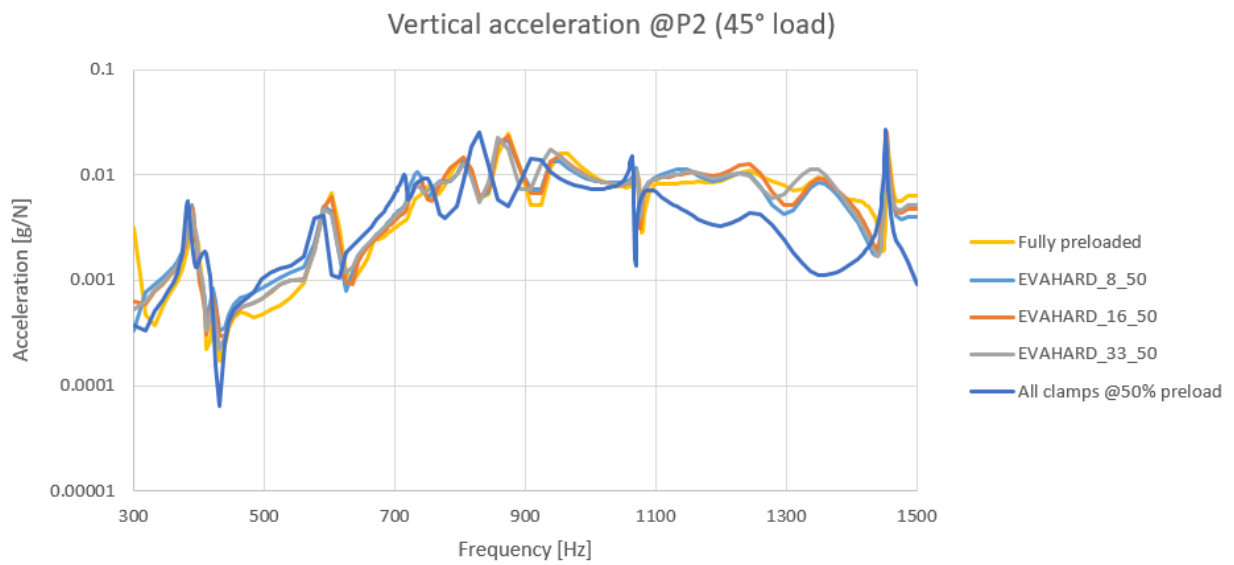


Figure 27 - Vertical accelerance spectrums when varying the number of half-preloaded clamps (45° load)

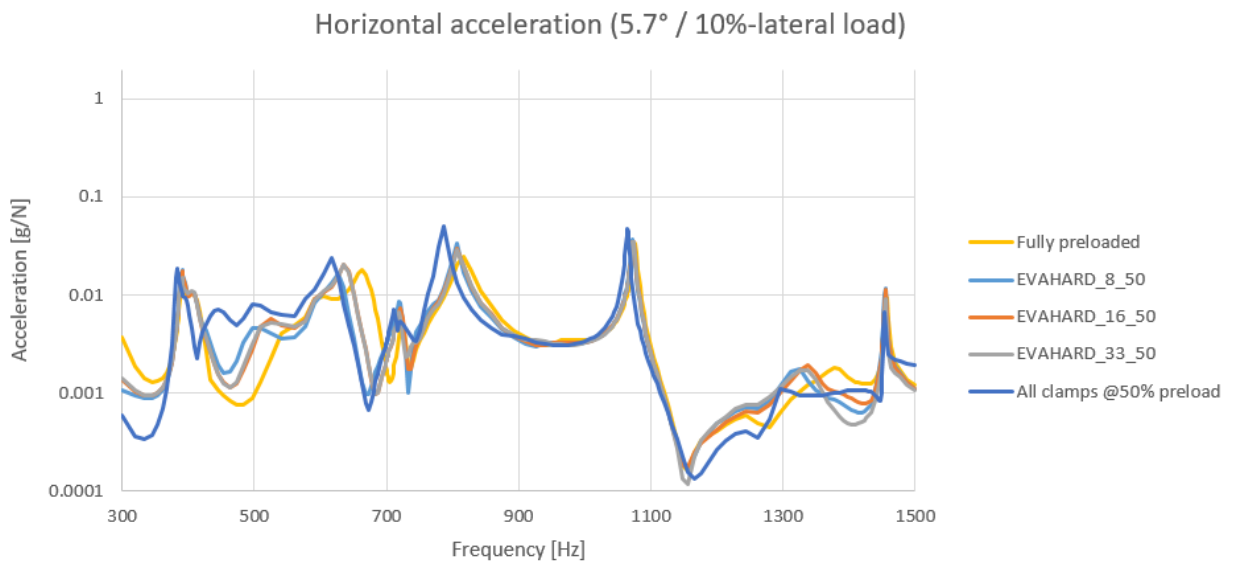


Figure 28 - Horizontal accelerance spectrums when varying the number of half-preloaded clamps (10%-lateral load)

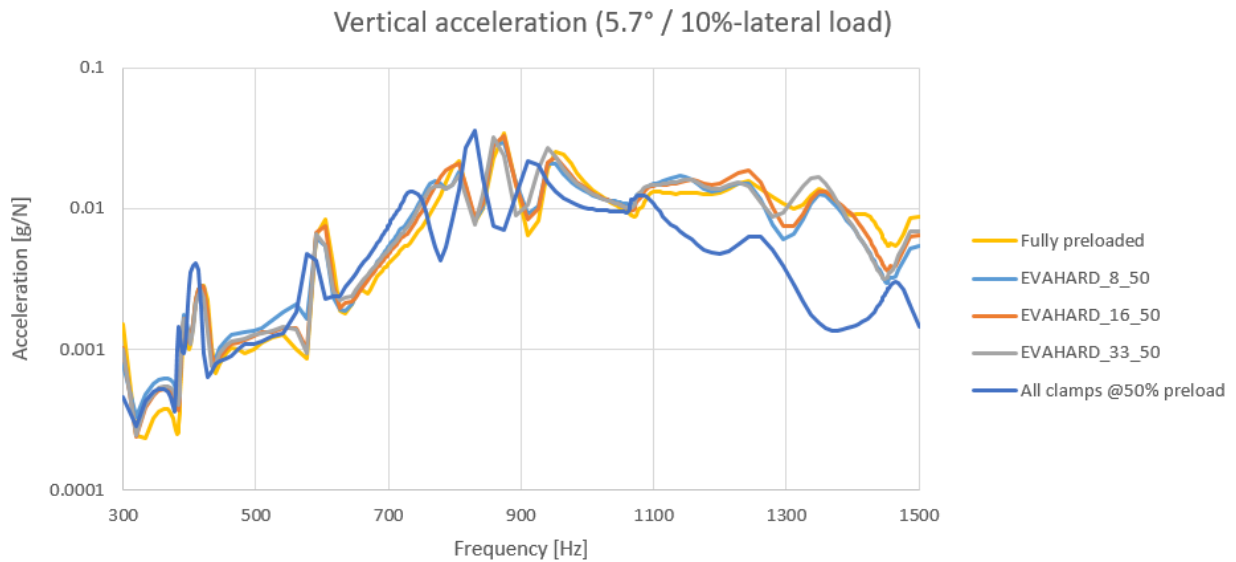


Figure 29 - Vertical accelerance spectrums when varying the number of half-preloaded clamps (10%-lateral load)

4.4 Acoustic results

In this section, the spectrums of the total emitted acoustic power are presented. Like in the experimental part, it is normalized by the input force squared.

4.4.1 EVA hard – all clamps with various loads

For the 45° load (Figure 30), the effect is clear again: all peaks increase when the preloads decrease. The graph on Figure 32 shows how the integral of the acoustic power over the frequency range (300 to 1500Hz) changes with preload. When decreasing the preload from 100% to 50%, the acoustic power increases linearly up to +1.65dB. However, for the 5.7° (10%-lateral load), Figure 32 shows the opposite. In Figure 31, some wide frequency bands seem to have their magnitude decreased when the preload decreases, while some others do not.

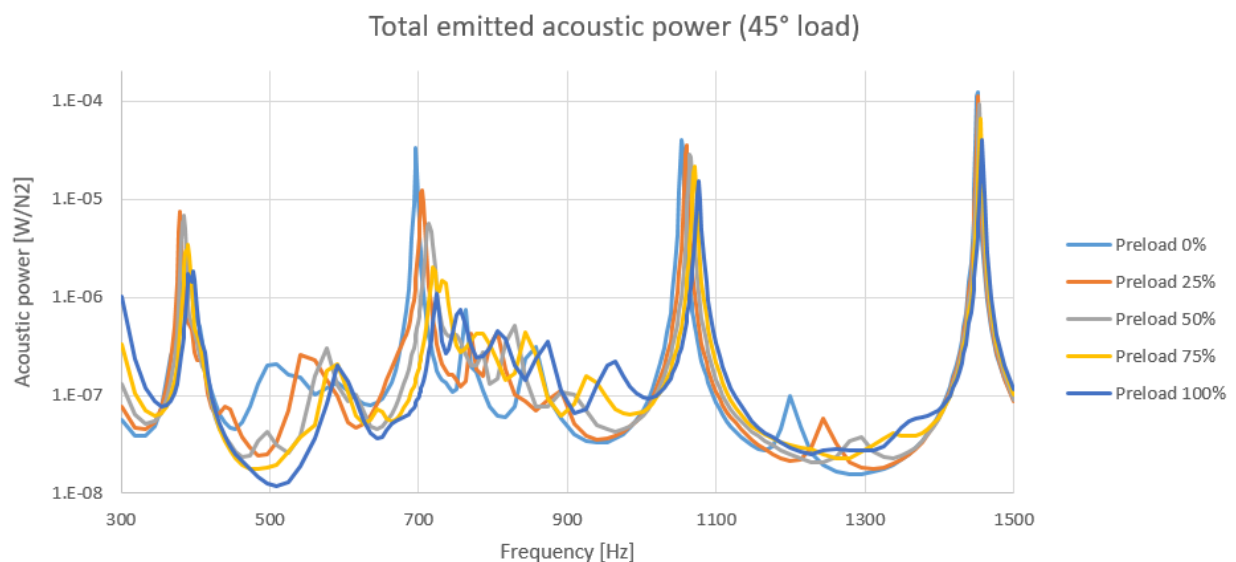


Figure 30 - Total emitted acoustic power (45° load)

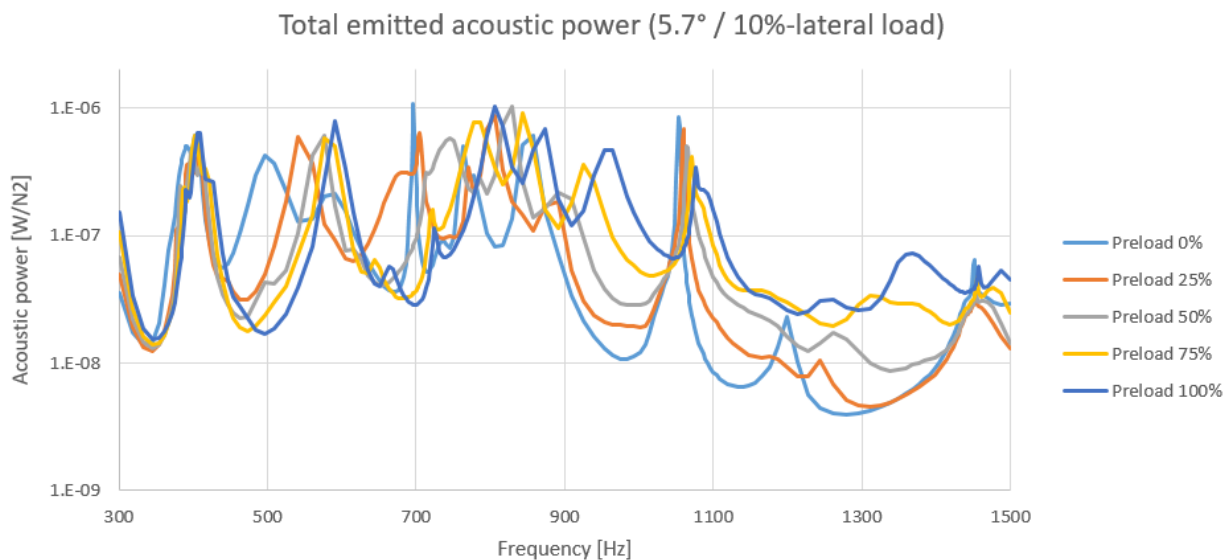


Figure 31 – Total emitted acoustic power (5.7° / 10%-lateral load)

The main difference between the two studied load directions is that with a 45° load, noise comes essentially from the rail vibrations (mostly lateral rail vibration modes of the excited rail), while the 10% lateral load excites all components relatively equally (coupled vertical rail-sleeper-ballast vibration modes). One can observe this on Figure 33, which shows the contribution of each component to the acoustic power for different frequency bands, based on the peaks locations. Note that the graph on the left is for the 45° load while the one on the right is for the 10% lateral load. The excited rail is always “railD” and the preload is 100%.

These diagrams also show that with 45° load, high frequency modes, corresponding to lateral rail vibration, are the most contributing to noise. On the other hand, with 10%-lateral, it is mainly the low to medium frequency modes that contribute to noise. Indeed, modes mostly involving the rails are generally at higher frequencies and are easily excited by lateral forces (45° loading). With a more vertical load, energy is mostly transmitted to the whole superstructure and coupled ballast - sleeper modes become as important as rail dominated modes.

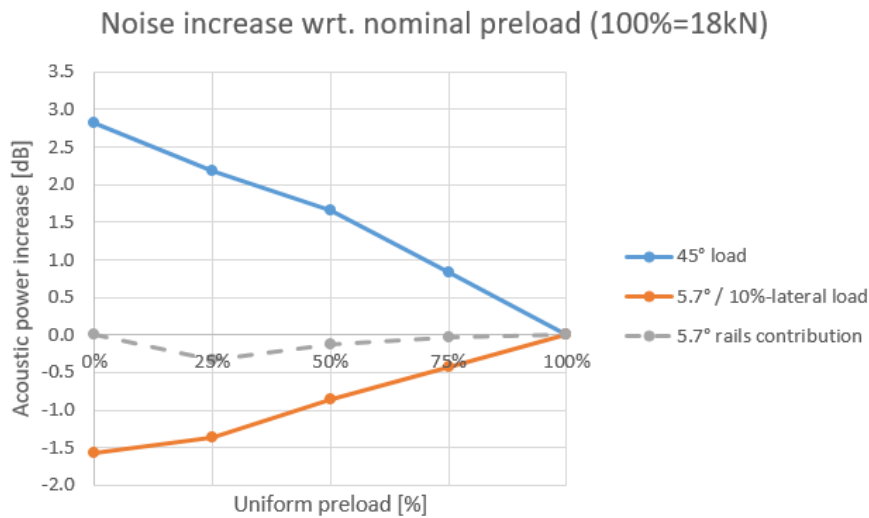


Figure 32 – Noise increase with respect to nominal preload (100%=18kN)

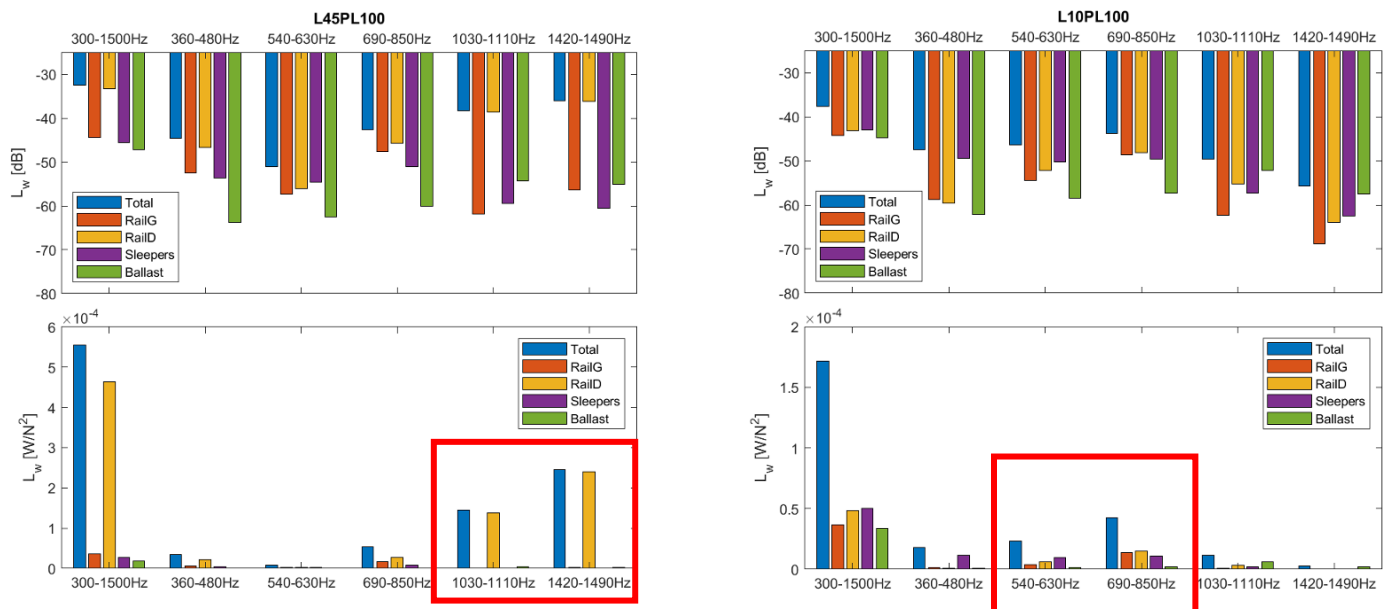


Figure 33 : Contributions of all components to the emitted acoustic power with 45° (left) and 5.7° load (right)

In the simulation of the 5.7° load case (mostly vertical) the overall noise decreases when the preloads decrease which is in opposition to the behavior with a 45° load case. These opposite trends can be explained as follows: Stiffer pads (i.e pads at higher preload) better transmit the rails vibrations to the sleepers and ballast which creates a strong coupling between the rails and the sleepers. For a 45° loading, stiffer pads tend to reduce the level of lateral rail vibration due to stronger coupling. As the rail is dominant in this loading case, the overall noise level is reduced in the case of stiffer pads or pads with higher preload (Figure 32).

However, with 10% lateral load, the dominant vibration modes (for example, the pin-pin mode at 400Hz, Figure 34 below), are coupled to strong sleeper bending modes. By increasing the preloads, railpad become more efficient at transmitting rail excitation to the sleepers, which then vibrate and radiate more. In this model at 10% lateral load, the higher the rail to sleeper coupling (high rail pad preload) the higher becomes the sleeper & ballast noise radiation contribution, which explains the trend shown in Figure 32). Note that all peak-wise charts, along with the associated operational shapes, are available in Appendix 7.5.4.

It must be noted that on a real rail track, sleepers are constrained laterally by the ballast which, by the way, is mechanically much more complex than the wooden beams modelled here. So it is expected that compared to a real track, the FE model give better noise emissions predictions when most of the contributions come from the rails, namely with a 45° load. Since in reality, sleepers and ballast radiate certainly way less noise than predicted here, the noise contribution of the rails alone was added to the graph in Figure 32. One can expect this gray curve to better predict overall trend in noise emissions for a real track. Despite still being negative, the noise level differences with respect to nominal preload are so small (<0.5dB) that they are negligible.

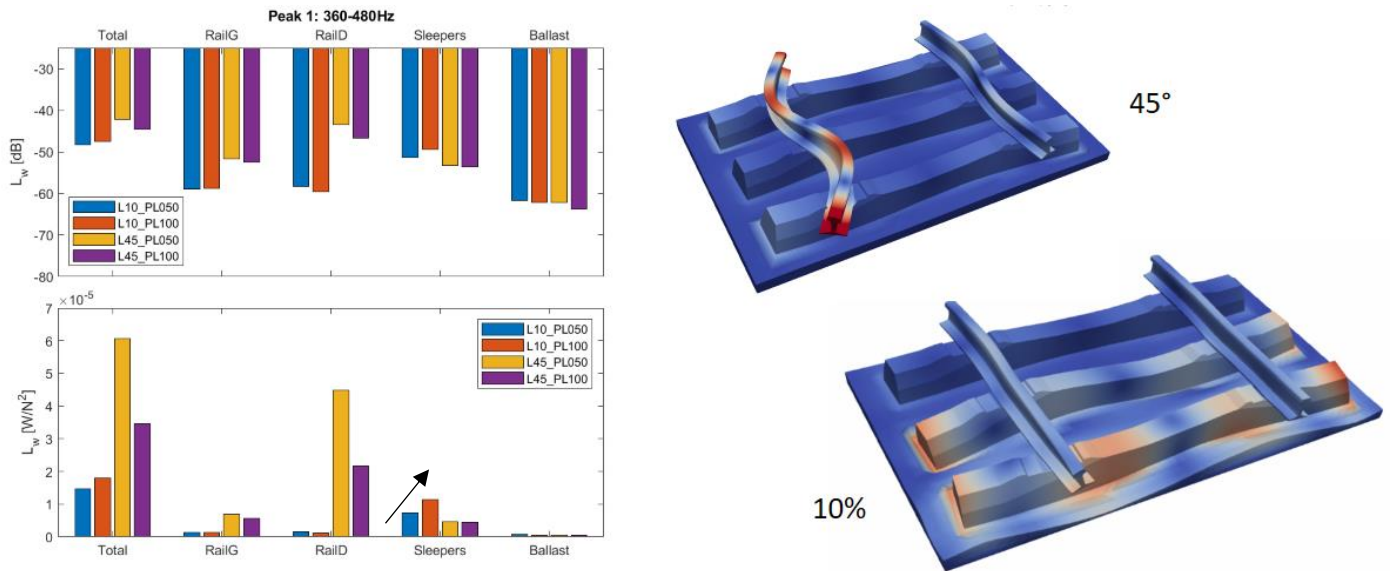


Figure 34 - Contributions to noise of each component around 400Hz (left) ; operational shapes at 400Hz (right)

To conclude, the model shows that the verticality of the 5.7° (10% lateral) force excites more easily the whole superstructure than the 45° force. Hence, all components play an important role in noise emissions. Stiffer pads (or higher preload) better transmit the vibrations of the rails to the rest of the superstructure which tend to radiate more noise. But since, in reality, sleepers vibrate much less thanks to the ballast constraining them laterally, the pads preloads would have a much less significant effect on noise levels, which is approximated here by ignoring the ballast and sleepers contributions. On the other hand, the 45° load shows a clear increase in noise emissions when the pads preloads are decreased, because the emissions mainly come from the rails.

As mentioned previously, compared to the experimental measurements, the simulation results show a stronger sensitivity to the preload than that of the experiments. This difference highlights that the modeling assumptions made in the model for the dependance of the railpad dynamic stiffness as a function of preload is probably overestimated compared to reality. It seems thus that the dynamic railpad stiffness does not decrease as much as its static stiffness when preload is reduced from 100% down to 25%. More advanced experimental characterization of the dynamic stiffness of the pads at different levels of preload would be needed to improve the accuracy of the model predictions.

4.4.2 EVA hard – various occurrences of a 50% preload

Figure 36 below are shows the spectrums of the simulated emitted acoustic power for partially un-tightened fasteners with a 45° loading. The green curves, “all clamps @50% preload”, are equivalent to EVAHARD_100_50 and show a distinct increase in amplitude of all peaks compared to the nominal case (“all clamps fully preloaded”, blue curves). Comparatively, when 8% to 33% of clamps are half-preloaded, the variation with respect to the nominal case is relatively small.

As for the 5.7° load (Figure 37), one can see that gradually setting a 50% preload to more clamps does not change the amplitudes linearly. At some frequencies, 16% of half-preloaded clamps induce higher peaks than 8%, which induce higher peaks than 33%.

The change of the total acoustic power compared to the nominal case is presented in Figure 35. In the case of 8 to 33% of the clamps with 50% preload the noise radiation increases with 45° load and decreases it with 10% lateral load according to the model. The model predicts maximum increase of radiated noise of +0.8dB for a 45° load and small reduction of less than 0.5dB for a 5.7° load direction.

As discussed before, with the current modeling assumptions on the rail pad stiffness, the model tend to over predicts the effect of the preload compared to experiments. Even so, when one third of the clamps are half-preloaded, the variation of predicted noise level is less than between +0.7 and -0.3dB. In a more realistic track setup, where ballast would damp the sleeper vibration more effectively, an even smaller effect would be expected. Overall as long as more than two thirds of the clamps are fully preloaded, the system keeps behaving the same way as if all clamps were fully preloaded.

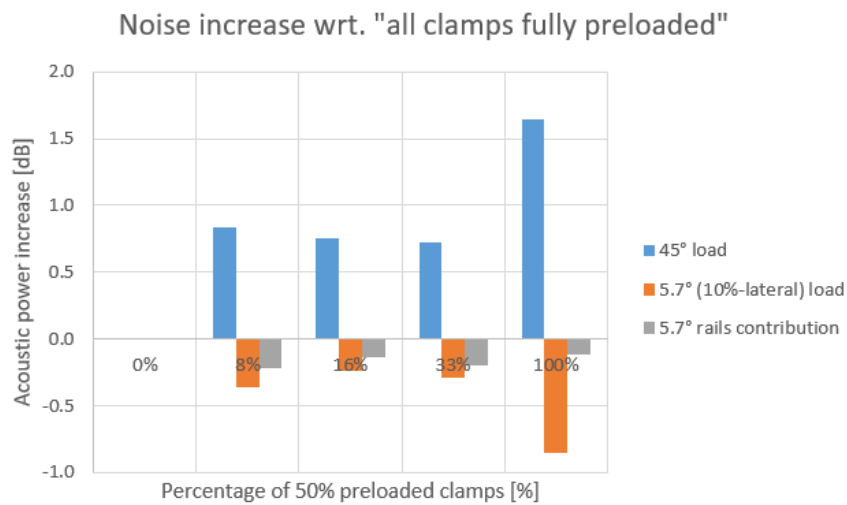


Figure 35 - Noise increase when some clamps are half-preloaded

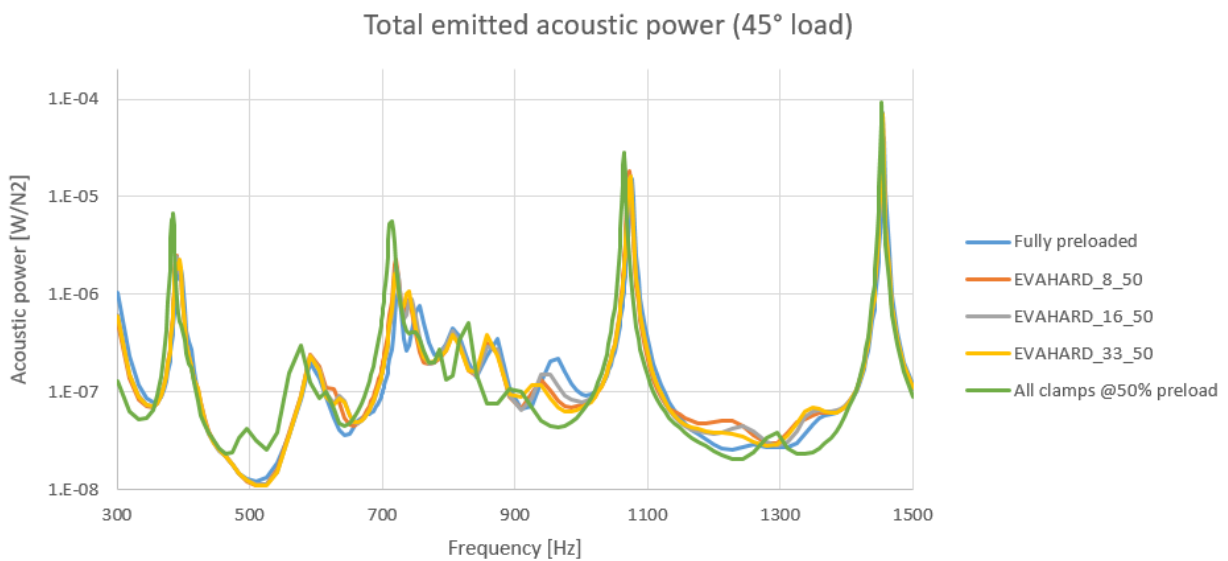


Figure 36 - Total emitted acoustic power (45°)

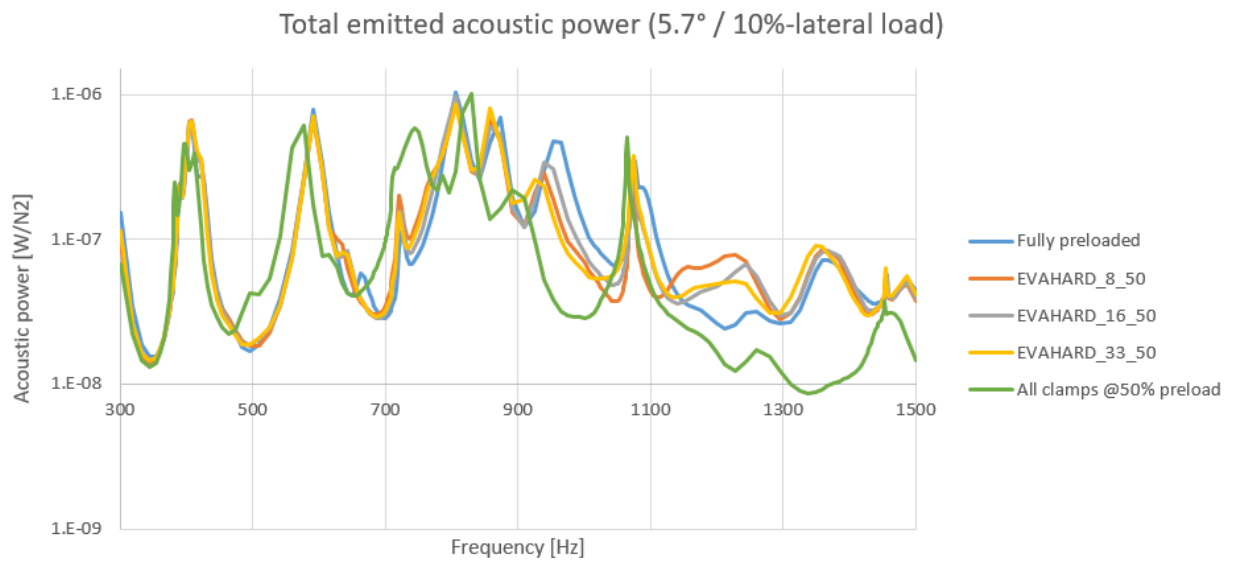


Figure 37 - Total emitted acoustic power (10%)

5 Discussion & conclusion

5.1 Synthesis

For the whole study three main case have been studied:

1. EVA hard pads with *all clamps* completely tightened to completely loose (100%, 75%, 50%, 25% or 0% of the nominal preload).
2. EVA hard pads with *1, 2 or 4 clamps* partially loose (8%, 16% and 33% of the clamps at 50% of the nominal preload).
3. EVA soft pads with *1, 2 or 4 clamps* partially loose (8%, 16% and 33% of the clamps at 50% of the nominal preload).

The following paragraphs synthesize the main results from the study.

5.1.1 Experimental

5.1.1.1 *Vibration measurements*

The first loading scenario shows no differences in the lateral accelerance of the rails, for all preload levels except when the clamps are completely loose. When the clamps impose no preload, the accelerance increases significantly, especially on the frequency range from 450Hz to 850Hz. For the vertical accelerance, vibrations at low frequency (300-500Hz) follow the same pattern.

Concerning the second and third loading scenarios, no notable differences are visible when 8, 16 or 33% of the clamps are at 50% preload. A similar observation is made for both EVA hard or soft pads.

5.1.1.2 *Acoustic measurements*

Under the first loading scenario, as for the vibration measurements, the noise emissions are not significantly affected by the preload level, except when there is no preload at all. In this case, the overall noise increases by about 2dB. The level of the peak at 1400Hz seems to decrease with reduced preload. However, this effect remains not very significant due the low coherence of the measurement above 1100 Hz in this setup.

For the other two scenarios, where 1, 2 and 4 clamps are preloaded at only 50%, there is no significant influence on noise emissions, whether for hard or soft EVA pads compared to the nominal case. Over the frequency range of 350 to 1100 Hz where the measurements exhibit a good coherence, the observed differences are at maximum +/-0.3dB. This small contrast is comparable to the level of reproducibility in this test setup.

Under a 5.7° excitation (instead of 45°), which is more representative of an actual railway track, no significant influence of the preload on the noise emissions could be found.

5.1.1.3 *Impact tests*

The first loading scenario shows a thresholds pattern: no significant differences between 100% preload to 25% preload, and an increase in measured displacement when clamps are completely loose (0% preload). The two other scenarios are similar: no significant differences, eventually a slight displacement increase when more clamps are preloaded at 50%.

5.1.2 Simulation

The vibro-acoustic FE model shows that uniformly decreasing the clamps preload transmits less vibrations from the rails to the rest of the superstructure. Consequently, the rails tend to vibrate more, hence more noise is radiated. This is particularly verified with a 45° load because the largest part of the noise is radiated by the rails. In this case, the model predicts up to 2.7dB increase in radiated noise when all clamps a loosened.

As for the 5.7° (10% lateral) load, the model predicts noise to be radiated almost equally by all track components because of the verticality of the exciting force. When uniformly decreasing the clamps preloads, the decrease of sleepers vibrations seems to compensate the rails vibrations increase which lead to a reduction of the predicted noise level up to -1.5dB. But on a real rail track, sleepers are laterally constrained by the ballast and their vibrations are much lower. So, if only the rails contribution to noise is taken into account, uniformly varying the clamps preloads has no significant effect on noise emissions with the 5.7° load (less than 0.5dB).

When only some clamps are unloaded (up to 33% of clamps having their preload halved), the effect on noise radiation is very low (order of magnitude: $\pm 0.5\text{dB}$). This is probably due to the other fully preloaded clamps, which are numerous enough to bear vibrations transmissions and make the system behave as if all clamps remained fully preloaded.

Overall, compared to the experimental results, the effect of preload is over represented in the current simulations. This mismatch is due to the assumptions made about the evolution of the dynamic pad stiffness with respect to preload which is considered similar to the evolution of the static stiffness. The observed mismatch between model and experiment shows that in reality, the dynamic pad stiffness is much less affected by preload than its static stiffness at least for the relatively stiff EVA pads considered in this study.

5.2 Conclusion

This study was performed on a three-sleeper unit cell with a substitute ballast in laboratory conditions. Therefore, the results obtained herein should be interpreted mostly as an indicator of the what could happen to a real continuous track but cannot represent exactly all the possible effects. Furthermore, most of the experimental part was performed with a 45° angle for the loading, which is a worst case scenario in terms of loading conditions (5.7° being more realistic). Despite those aspects, the set-up is in a 1:1 scale, real sleepers, pads and rails are used.

The study shows no significant difference of acoustic emissions when all the clamps are preloaded between 100% and 25% of the nominal preload. However, when all the clamps are completely loose (0% of the nominal preload), acoustic emissions increase significantly.

A more realistic scenario where only a few clamps are untightened, 1, 2 or 4 clamps (8%, 16% and 33% respectively) at 50% of the nominal preload shows no significant differences in acoustic emissions. Those tests have been repeated on both hard and soft EVA pads from SBB, and the conclusion remain unchanged.

Acoustic measurements performed with a more realistic 5.7° loading did not show significant influence of the clamps preload on acoustic emissions either.

Concerning the numerical model of the three-sleeper unit cell, it was especially useful to give a better understanding of the rail track dynamics by looking at how it deforms and how each component contributes to noise emissions. Overall the model tended to overpredict the effect of preload which lead to the observation that the dynamic stiffness of the EVA hard & soft pads is much less affected by preload than its static stiffness. Thus to improve the simulation accuracy, the dynamic stiffness of the pad should be measured at high frequency for different preloads.

Some other aspects of clamping preload could not be studied herein but could have a potential effect in a real track:

- Dynamic force: Indeed, we considered here that the dynamic excitation force is not dependent on the preload, while in reality, the complex wheel-rail-pad-sleeper interactions could potentially be affected by a reduced preload.

- Partial sleeper contact / differential settlement: In the present setup all three sleepers were in perfect contact with the simulated ballast and thus no sleeper was “floating” as it can happen in reality. Moreover, a loose clamping system could potentially be a cause for a differential settlement of the ballast under the sleeper. A loose clamping system could modify the impulse and vibrations transferred to the ballast and thus modify the rate of ballast settlement under that particular sleeper compared to the others. Such variability could lead to a loss of contact of the sleeper with the ballast and would lead to a significant degradation of the track condition and probably a strong increase in noise.

6 References

1. Die Bundesversammlung der Schweizerischen Eidgenossenschaft. *Bundesgesetz über die Lärmsanierung der Eisenbahnen*. Bern : s.n., 2014.
2. KPZ Fahrbahn ; Huber, Philipp ; Schneider, Philippe. *Forschungsprojekt Schienenbefestigung Phase I - Schlussbericht*. s.l. : FOEN, 2021.
3. Arbeitsgruppe VöV. *Handbuch Fahrbahnpraxis Normalspur D RTE 22040*. Bern : VöV, 2010.

Appendices

7.1 Clamp preload adjustment

The Wk 14 clamps are linear springs designed for a nominal preload of 9kN. They are linear springs, meaning that their deflection is strictly proportional to their preload. In order to be correctly tightened, the air gap (Luftspalt) between the central part of the clamp and the angle guide plate must not exceed 0.5mm.

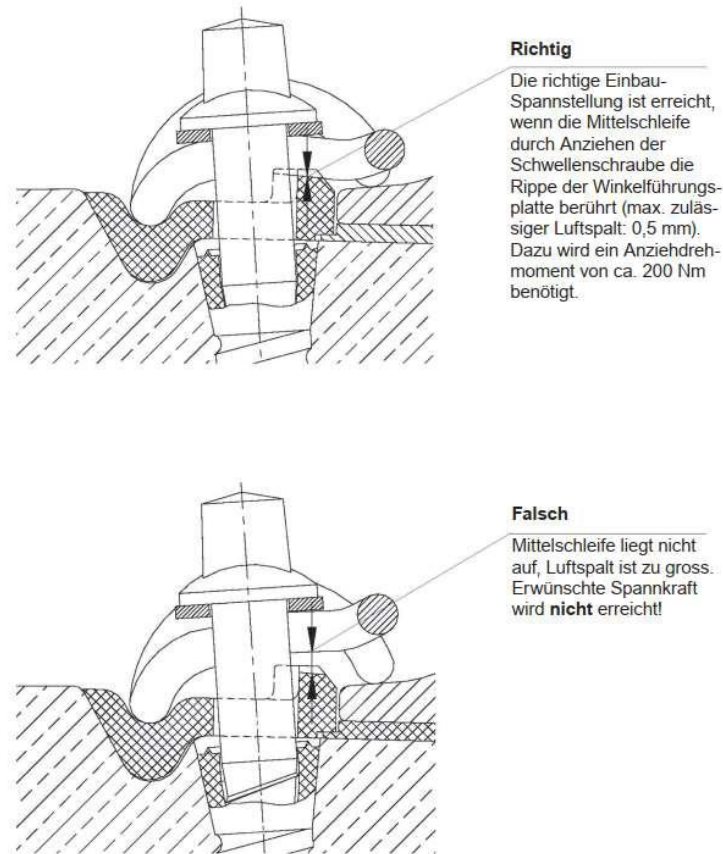


Figure 38 - Clamp tightening guidelines (3)

The deflection of the spring has been chosen as the reference parameter to adjust the load of the springs, because it is repeatable and representative of the actual preload of the clamp. As stated in the FOEN/KPZ study (2), the tightening torque is not a reliable indicator of the clamp preload, as it is too much dependant of the friction in the screw system. This was also observed on the unit-cell setup, where a “clean” clamp and a rusted one, both tightened with the same torque, didn’t have the same air gap. In order to measure the air gap, and thus the preload, the total deflection span (approximately 10mm with a 7mm pad) of the middle bend of the clamps has been measured as the difference between its highest (no load) and its lowest (maximum load) position, relatively to the sleeper. The position of the clamp middle bend relatively to its lowest position approximately equals the air gap between the clamp and the angle guide plate, as the clamp is seated in the angle guide plate when at its lowest position. To get the desired preload, the clamp tightening is adjusted until the desired deflection is attained, with a precision of $\pm 10\%$.

The FOEN/KPZ study determined that about 15 % of clamps present an air gap greater than 2mm. In the present study, the 50% loading case, corresponding to an air gap of about 5mm, was more investigated as it is more realistic than a totally loose clamp, and a bit worse and conservative than an air gap of 2mm.

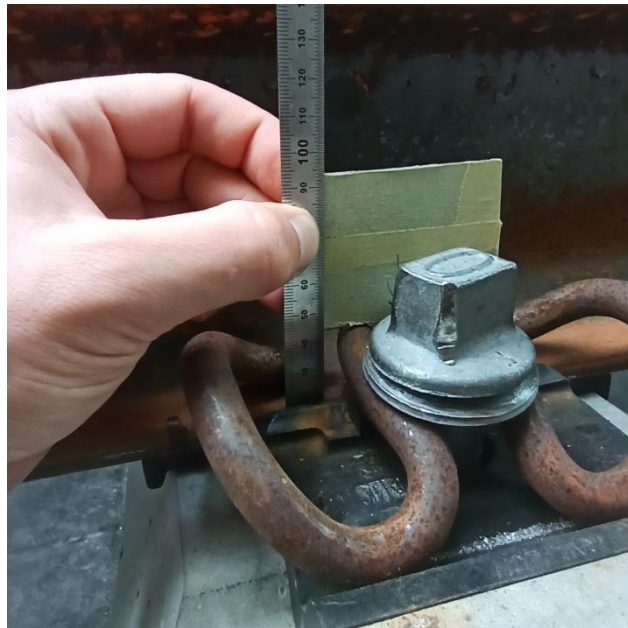


Figure 39 – Preload / air gap adjustment

7.2 Vibratory measurements

Vibratory measurements consist in exciting the system with a random harmonic force covering the whole frequency range of interest (called white noise). The input force and the acceleration at various points are measured.

There are mainly two ways of using the data acquired from a vibration measure:

1. To know the vibration pattern at a given frequency, see Figure 41.
2. To know the amplitude of vibration of a given measure point for the entire frequency spectrum, see Figure 40.

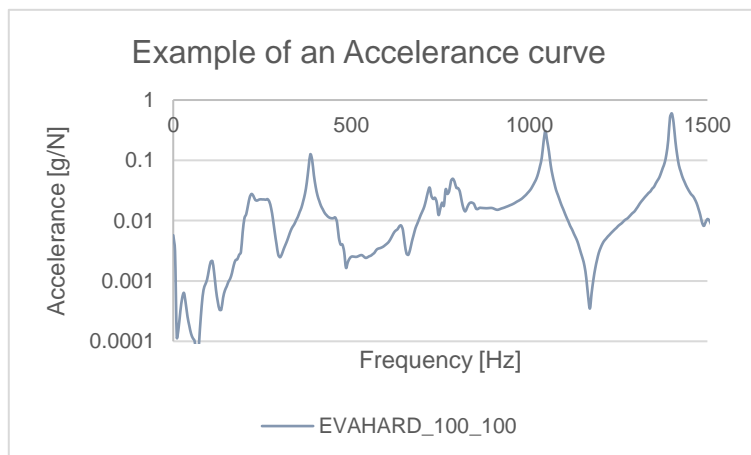


Figure 40 – Example of an accelerance spectrum for a given point.

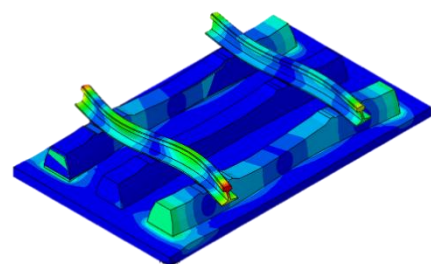


Figure 41 – Vibration pattern for a given frequency (390 Hz).

In this study, the data were analysed and compared focusing on two reference points by extracting the amplitudes normalized by the input force. All the measured points are represented on the Figure 42, the red dots show the location of the reference points, the upper one is number 31 and the lower one the number 30. They are located on the top of the excited rail, above the middle sleeper or at half-distance between two sleepers.

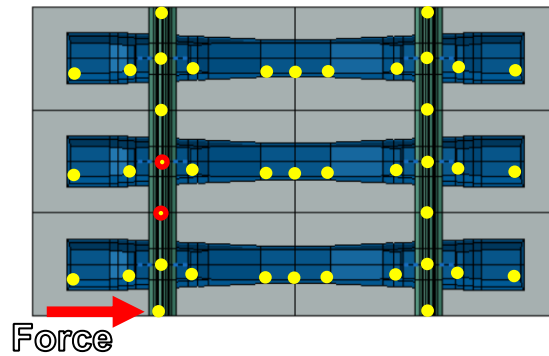


Figure 42 – Measure points for the vibratory measurements.

7.3 Acoustic measurements

7.3.1 Intensimetry method

The acoustic measurements were performed using the intensimetry method. Intensimetry is performed by placing a pair of microphones on various points along a surface enclosing the source of noise that is to be measured. At each point, the sound intensity (in W/m^2) is measured. The intensity data is then integrated over the surface area of the enclosing surface, to get the total emitted acoustic power (in W). In the present study, each sound intensity measurement is normalized by the exciting force squared (in N^2), to allow for comparison between different measurements as the force may vary slightly during a measurement as well as between different measurements.

One of the advantages of intensimetry is that constant background noises are suppressed. Concerning punctual acoustic perturbations, care is taken during the measurement process to avoid them, and data polluted by punctual perturbations is discarded.

The intensimetry results are given in the form of a spectral plot. For the whole spectrum (300-1500Hz) and for other discrete bands, the power levels are computed by integrating the spectral curve over the frequency ranges of interest. The obtained levels are then displayed in a table as well as in a bar graph view.

7.3.2 Repeatability and error

In order to know the reliability of the measurements, several measurements of the same unit-cell configuration have been made. For each measurement, the power levels over the bands of interest are computed. The results are then mean-averaged for each band of interest. Finally, the maximal difference with respect to the mean is kept as the error of the band, for all further measurements. This allows to know which part of the spectrum are reliable.

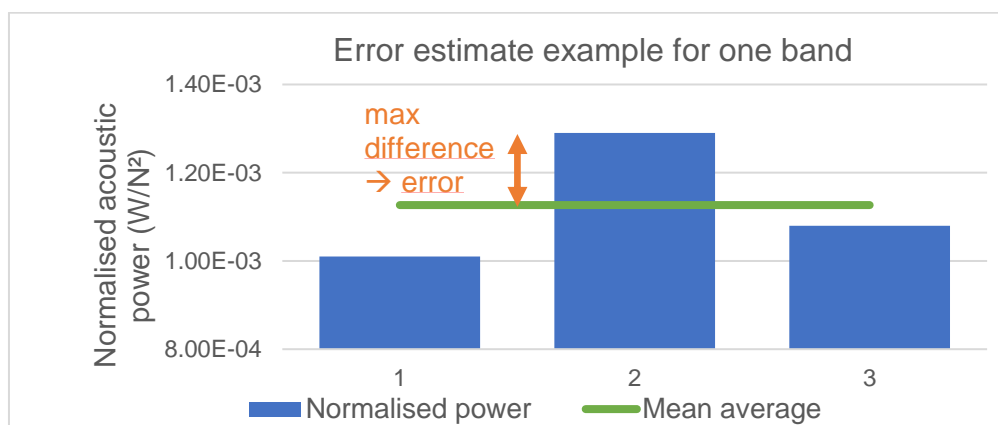


Figure 43 - Illustration of the calculation of the error bars of the histograms

7.3.3 Coherence

Another way to evaluate the reliability of the measurements is to compute the coherence of the data. The coherence answers the question: « how much does the output relate on the input ? ». The answer is a value between 0 (not related) and 1 (totally related).

The following graphs represent the coherence between the acoustic pressure (output) and the force (input) for various clamp loading cases. The areas in green highlight the frequency ranges where the mobile mean (on 60Hz) of the coherence is equal or superior to 0.6 (0.6 is the highest value which gave the highlighted parts a consistent range, between 350 and 1100Hz).



Figure 44 - Force to acoustic pressure coherence for various preloads

This means that outside the 350-1100Hz range, the measured sound pressure is less related to the excitation induced in the setup. This is also coherent with the error bars calculation, that show way less uncertainty in the 350-1100Hz range than in the 300-1500Hz range.

7.4 Impact measurements

The impact test consists of measuring the acceleration at various points following an impact on a rail. The impact is done with an instrumented hammer, which contains a load cell that records the force during the impact, Figure 46. The recorded acceleration, Figure 46, is then integrated two times to obtain the induced displacement. Finally, the displacement is normalized by the force to compare the samples with each other's, Figure 47.

The Figure 45 shows the measure points (red dots) and the impact point (red arrow).

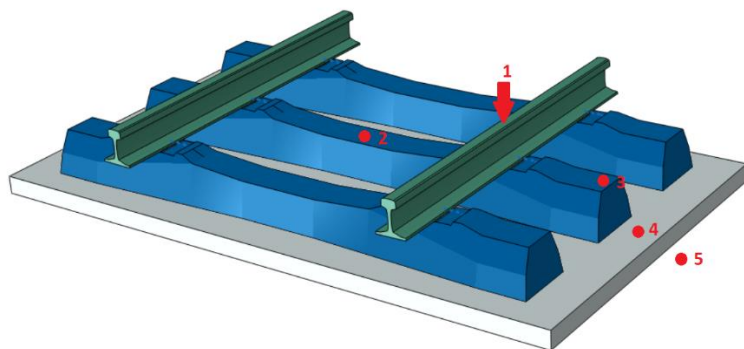


Figure 45 – Measure point location.

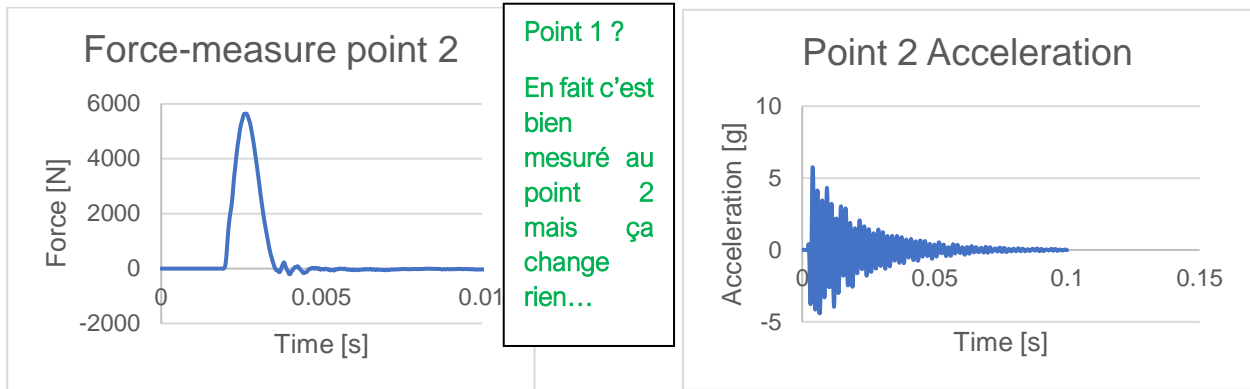


Figure 46 – Left : Impact force measured ; Right: Acceleration measured.

Point 1 ?
En fait c'est bien mesuré au point 2 mais ça change rien...

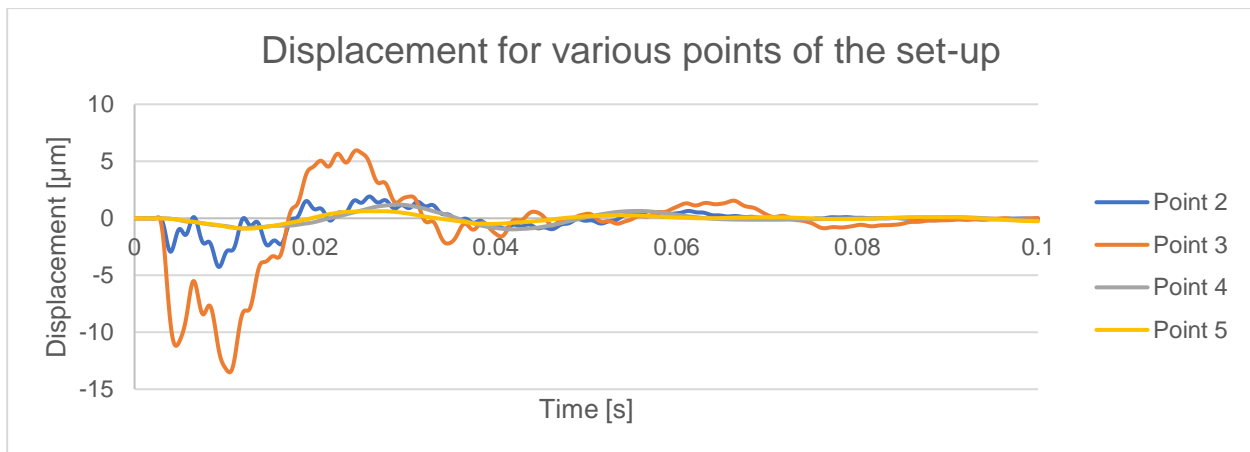


Figure 47 – Displacements for various point on the unit-cell after an impact.

7.5 Simulations

7.5.1 Materials properties

The Table below summarizes the materials properties used for all materials in the model. As for Young's modulus and damping coefficient of EVA, their evolution with respect to frequency is presented in Figure 48. The data points come from Dynamic Mechanical Analysis and they were linearly fitted in the range of interest from 300 to 1500Hz. Note that even though the damping coefficient of EVA is nearly constant, a linear fitting was used anyway because the model treats pads materials mechanical properties as frequency-dependant.

	Wood (Ballast)	Concrete (Sleepers)	Steel (Rails)	EVA (Pads)
Young's modulus E [GPa]	0.05	46.3	210	
Damping $\tan\delta$ [-]	0.04	0.016	0.001	
Density ρ [kg/m ³]	520	2435	7850	1000
Poisson's ratio ν [-]	0.3	0.2	0.3	0.484

Table 1 - Materials properties used in the model

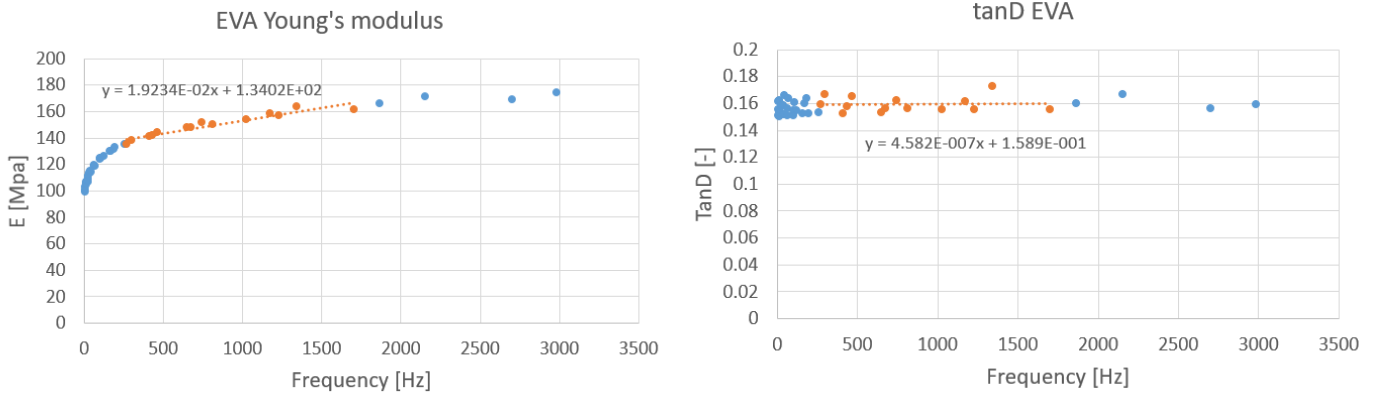
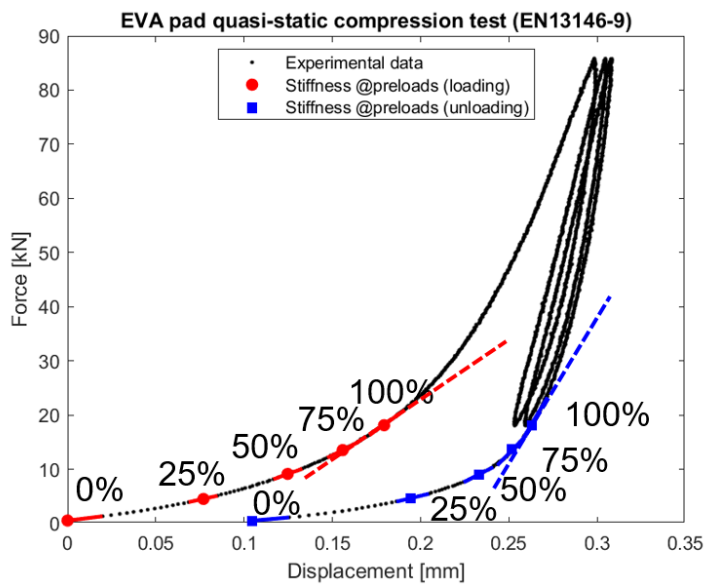


Figure 48 - Mechanical properties of EVA

7.5.2 Preload modelling

Figure 49 shows the force-displacement curve of a quasi-static compression test for a hard EVA pad. Since the slope at a given point (preload state) is the tangent stiffness, it is clear that decreasing the preload decreases the pad stiffness. This is mainly due to the high level of confinement and the quasi-incompressibility of the pads. Therefore, a simple way to implement preload variation is to tune Young's modulus of EVA in the model parameters.



Preload [%]	Coefficient [-]
0	0.113
25	0.228
50	0.406
75	0.665
100	1

Table 2 – Preload coefficients

Figure 49 - EVA pad quasi-static compression test

At each preload state from 0% to 100% (0 to 18kN), the effective Young's modulus of EVA can be computed as $E_{eff} = \alpha \cdot E_{100\%}$ where α is the ratio between the slope of the force-displacement curve at some preload and the slope at 100% preload. The coefficient obtained must take into account the stiffness differences (due to hysteresis) between loading and unloading by averaging the values obtained along both paths.

7.5.3 Acoustic computation

Acoustic pressure waves are generated because of the rail track vibrations. Every part of the superstructure (especially the rails) acts like speakers, moving air back and forth as it vibrates in the whole spectrum of the input force. At each frequency, harmonic simulations provide the displacement, velocity and acceleration fields over the whole model.

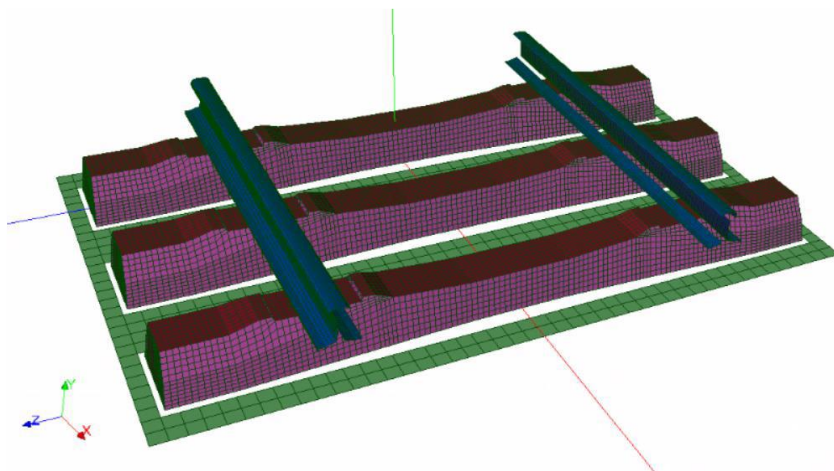


Figure 50 - Set of radiating surfaces

A set of radiating surfaces (Figure above) is chosen among the external surfaces of the mesh. If every point of these surfaces is considered as a perfect monopole acoustic source, the superposition of all points contributions allows the computation of the acoustic pressure at any point in space. The peak pressure of a monopole source can be computed as

$$p(r) = \frac{\rho c k v_{\perp} S}{4\pi r}$$

where $\rho = 1.21 \text{ kg/m}^3$ and $c = 343 \text{ m/s}$ are respectively the air density and speed of sound, $k = 2\pi f/c$ is the wave number, v_{\perp} is the velocity component normal to the vibrating surface and S is the surface area.

The principle of monopoles superposition is valid at a distance greater than about four times the characteristic distance of the model. So, the pressure field is computed over a 7m-radius hemisphere, whose mesh is fine enough (400 evenly spread points) to capture all high pressure zones at any frequency. The intensity field $I = p^2/\rho c$ is then spatially integrated to obtain the acoustic power spectrum.

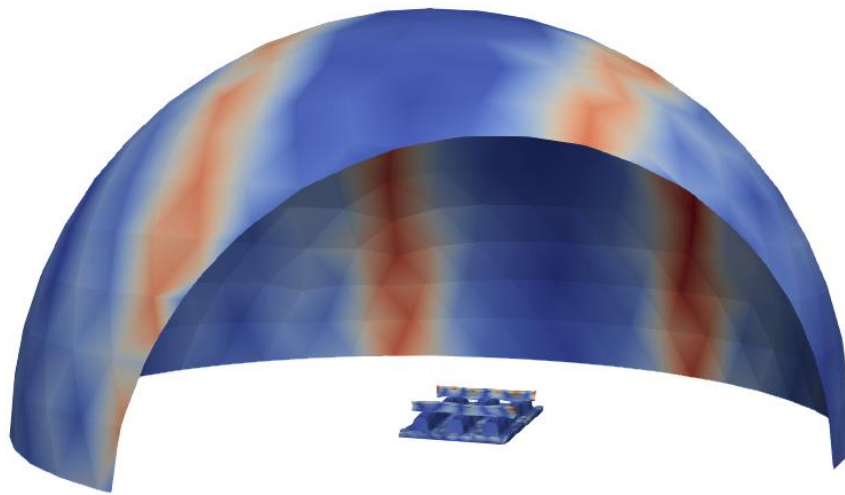


Figure 51 - Hemispheric surface used for pressure field computation

7.5.4 Peak-wise acoustic results

Below are shown the contribution to the radiated noise of each component: rails (“railD” is the excited rail), sleepers and ballast. They were simulated for four cases: the two load directions (10% and 45°) and two uniform preloads (50% and 100%). The first Figure shows the results for the whole frequency range and how the frequency bands were selected. The other figures are peak-wise. The name of the series is “LXX_PLYYY” where XX takes the value “10” or “45” and denotes the load orientation and YYY takes the value “050” or “100” and designates the preload in percentage.

